Advanced Polymer Architecture for Preparation of Hairy Single-Walled Carbon Nanotubes

ADVANCED POLYMER ARCHITECTURE FOR PREPARATION OF HAIRY SINGLE-WALLED CARBON NANOTUBES

BY

UNNATI DESAI, B.SC.

A THESIS

SUBMITTED TO THE SCHOOL OF GRADUATE STUDIES

OF MCMASTER UNIVERSITY

IN PARTIAL FULFILLMENT OF THE REQUIREMENTS

FOR THE DEGREE OF

M.SC. IN CHEMISTRY

© Copyright by Unnati Desai, 2025 All Rights Reserved M.Sc. of Chemistry (2025)

McMaster University

(Chemistry and Chemical Biology)

Hamilton, Ontario, Canada

TITLE: Advanced Polymer Architecture for Preparation of

Hairy Single-Walled Carbon Nanotubes

AUTHOR: Unnati Desai

B.Sc. (Chemistry)

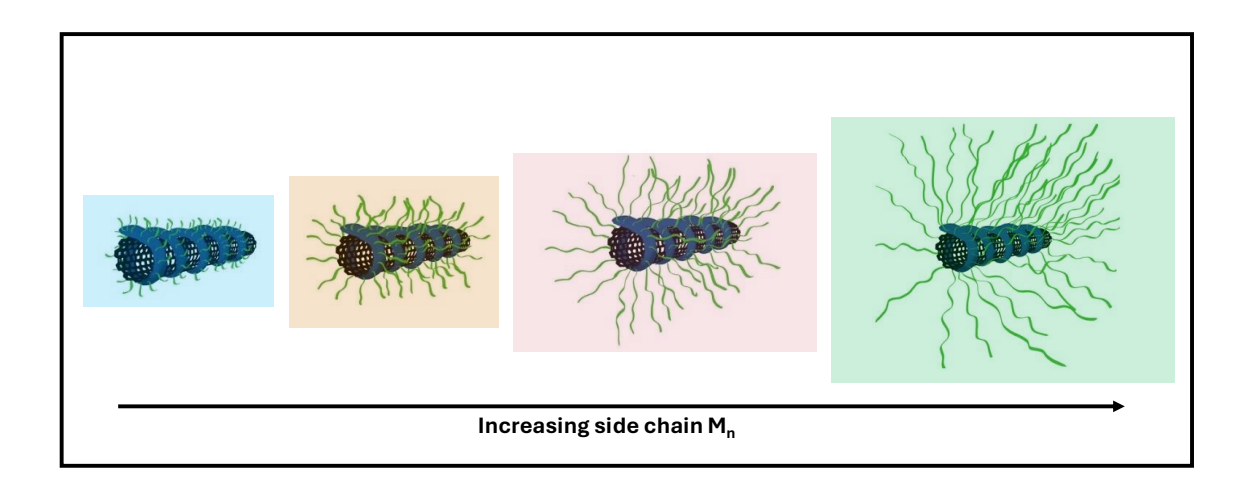
Toronto Metropolitan University, Toronto, ON, Canada

SUPERVISOR: Professor Alex Adronov

NUMBER OF PAGES: XVI, 73

Abstract

Advanced polymer architectures present new opportunities for single-walled carbon nanotube (SWNT) functionalization resulting in intriguing supramolecular structures. Graft copolymers, in particular, possess distinctive properties from their linear analogues. Their unique self-assembly behaviour and conformational variations are of specific interest. Herein a series of poly(fluorene)-g-poly(ethylene glycol) graft copolymers are used to prepare dispersions of SWNTs, first in THF then through solvent exchange in water. Using strain promoted azide alkyne cycloaddition, various molecular weights of mPEG chains (5, 10, 20 and 40 kDa) have been grafted onto a poly(fluorene) backbone. Atomic Force Microscopy shows that increase in side chain degree of polymerization results in distinct conformational differences between each graft copolymer leading to subsequent unique architectures of SWNT dispersions.



Acknowledgements

Without the encouragement and support from Professor Alex Adronov, earning this degree would have been a much more difficult journey. Thank you, Alex, for encouraging me to trust myself and my abilities and for allowing me the space to learn from both my mistakes and the process of overcoming them.

Thank you, also, to my committee members Dr. Katherine Bujold and Dr. Anthony Rullo who have provided me with such insight and guidance.

I would be remiss to forget my friends and colleagues in the Adronov Group, past and present who I have been lucky to learn from and learn with. I'll miss our coffee walks and chats in the office. I also want to acknowledge all the people who have trained me and TA'd with me, who spent a few extra minutes explaining new concepts or provided insight, encouragement and humour. My time in the Adronov Group and at McMaster may have been short but it was profoundly valuable and memorable.

Lastly, I want to thank my family. Although they may not be able to explain the crux of my thesis, they can certainly detail the long days, late nights and breadth of work it took to accomplish it. All of which is thanks to their unwavering support.

Over the past two years I've been fortunate to learn from so many different people. More than a degree, there are countless lessons in chemistry and beyond that I will take with me as I leave McMaster. I'm (graft)eful for it all.

Table of Contents

Abstract	iii
Acknowledgements	iv
List of Abbreviations	viii
List of Tables	xi
List of Supporting Tables	xi
List of Figures	xii
List of Supporting Figures	xiv
List of Schemes	xvi
Chapter 1: Introduction	1
1.1 Single-Walled Carbon Nanotubes (SWNTs)	1
1.2 SWNT Properties	1
1.3 Synthesis of SWNTs	4
1.3.1 Arc-Discharge	4
1.3.2 Laser Ablation	5
1.3.3 Chemical Vapour Deposition (CVD)	5
1.3.4 Variations of CVD	6
1.4 Functionalization of SWNTs	7
1.4.1 Covalent Functionalization	8
1.4.2 Non-Covalent Functionalization	9
1.4.3 Aqueous Dispersions of SWNTs	11

1.5 Characterization Techniques	12
1.5.1 Atomic Force Microscopy (AFM)	12
1.5.2 UV-Vis-NIR Spectroscopy	15
1.5.3 Resonance Raman Spectroscopy (RRS)	16
1.5.4 Thermogravimetric Analysis (TGA)	19
1.6 Graft Copolymers	19
1.6.1 Bottlebrush Polymers (BBPs)	20
1.6.2 Comb vs Bottlebrush Polymers	23
1.7 Graft Copolymer Synthesis	24
1.7.1 Grafting-through Method	25
1.7.2 Grafting-to Method	25
1.7.3 Grafting-from Method	26
1.8 Summary	27
Chapter 2: Advanced Polymer Architecture for Preparati	on of Hairy Single-Walled
Carbon Nanotubes	28
2.1 Synthesis of Backbone	28
2.1 Synthesis of Dackbone	20
2.2 Synthesis of Side Chains	31
2.3 Strain Promoted Azide-Alkyne Cycloaddition	
2.3 Strain Promoted Azide-Alkyne Cycloaddition 2.4 Characterization of Graft Copolymers	32
	32
2.4 Characterization of Graft Copolymers	
2.4 Characterization of Graft Copolymers	

2.5 Preparation of PF-PEG-SWNT Dispersions	38
2.5.1 Determining Equal Concentration of Backbone Polymer	. 38
2.6 Characterization of SWNT Dispersions	41
2.6.1 UV-Vis-NIR Spectra of SWNT Dispersions in Water and THF	. 42
2.6.2 Resonance Raman Spectra of SWNT Dispersions in Water and THF	. 43
2.6.3 Atomic Force Microscopy Images of SWNT Dispersions	. 44
Chapter 3: Conclusions and Recommendation for Future Work	47
3.1 Conclusion	47
3.2 Recommendation for Future Work	47
References	49
Appendix	58
A1 General Experimental	58
A2 Statistical Analysis	59
A3 NMR Spectra	60
A4 Gel Permeation Chromatography (GPC)	67
A5 AFM Images	68
A6 Calculations	69
A6.1 Theoretical Calculations for TGA Curves	. 69
A6.2 Extinction Coefficient and Mass Calculation of PF-N ₃ in Graft Copolymers	. 70

List of Abbreviations

1D One-Dimensional

3D Three-Dimensional

AFM Atomic Force Microscopy

ATRP Atom Transfer Radical Polymerization

BBP Bottlebrush Polymer

CDCl₃ **Deuterated Chloroform**

CNT Carbon Nanotube

Cobalt, Molybdenum Catalysis CoMoCAT

Cethyltrimethylammonium Bromide CTAB

CVD Chemical Vapour Deposition

Dibenzoclyclooctyne DBCO

DBCO-NHS Dibenzoclyclooctyne-N-hydroxysuccinimide

DCM Dichloromethane

DFT **Density Functional Theory**

DI water Deionized water

Deoxyribonucleic Acid DNA

M.Sc. Thesis – Unnati Desai McMaster University – Chemistry and Chemical Biology

DOS Density of States

FTIR Fourier Transform Infrared

GPC Gel Permeation Chromatography

¹H NMR Proton Nuclear Magnetic Resonance

HiPCo High-pressure Carbon Monoxide Disproportionation

HOMO Highest Occupied Molecular Orbital

HOPG Highly ordered pyrolytic graphite

LUMO Lowest Unoccupied Molecular Orbital

m-SWNT Metallic-Single-Walled Carbon Nanotube

mPEG Methyl-Poly(ethylene) Glycol

MWNT Multi-walled Carbon Nanotube

NMP Nitroxide-Mediated Polymerization

 N_{sc} degree of polymerization of side chain

pBA Poly(n-butyl acrylate)

PECVD Plasma Enhanced Chemical Vapour Deposition

PES Polyethersulfone

RAFT Reverse Addition-Fragmentation Chain Transfer

M.Sc. Thesis – Unnati Desai McMaster University – Chemistry and Chemical Biology

RBM Radial Breathing Mode

RRS Resonance Raman Spectroscopy

SC Sodium Cholate

sc-SWNT Semiconducting-Single-walled Carbon Nanotube

SDBS Sodium Dodecyl Benzene Sulfonate

SDS Sodium Dodecyl Sulfate

SPAAC Strain Promoted Azide Alkyne Cycloaddition

SWNT Single-walled Carbon Nanotube

TGA Thermogravimetric Analysis

THF Tetrahydrofuran

UV-Vis-NIR Ultraviolet-Visible-Near-Infrared

VHS van Hove Singularities

z Grafting density

List of Tables

TABLE 1. TABULATED MASS LOSS PERCENTAGES OF EACH GRAFT COPOLYMER AS DERIVED FROM TGA CURVES (FIGURE 14) ALONG
WITH THE CALCULATED THEORETICAL MASS LOSS PERCENTAGES36
TABLE 2. TABULATED MASSES OF GRAFT COPOLYMERS AND SWNTs ALONG WITH SOLVENT VOLUMES USED FOR PREPARATION OF
DISPERSIONS40
List of Supporting Tables
TABLE S1. TABULATED CONCENTRATIONS AND ABSORBANCES USED TO GENERATE THE TRENDLINE. 71
TABLE S2. TABULATED VALUES OF ABSORBANCES FOR EACH GRAFT COPOLYMER DETERMINED FROM UV-VIS SPECTROSCOPY AS
SEEN IN FIGURE 16 AND THE CORRESPONDING CONCENTRATIONS CALCULATED USING THE BEER LAMBER LAW
TABLE S3. TABULATED CALCULATED MASSES OF PF-N ₃ IN EACH SAMPLE OF GRAFT COPOLYMER IN THF

List of Figures

FIGURE 1. SCHEMATIC SHOWS UNROLLED (A) AND ROLLED (B) GRAPHENE SHEET OF A (4, 2) NANOTUBE. CONNECTION OF SITES
O and A and B and B' result in the rolled sheet (b). Roll-up vector $\mathbf{C}_{\!\scriptscriptstyle H}$ is expressed by vector OA and
TRANSLATIONAL VECTOR T IS EXPRESSED BY VECTOR OB. 17 REPRINTED FROM PHYSICS REPORTS, 409, DRESSELHAUS,
M.S., ET AL., 47-99, COPYRIGHT (2005), FROM ELSEVIER 2
FIGURE 2. ILLUSTRATION OF THE DENSITY OF STATES (RIGHT) OF A (4, 20) NANOTUBE DERIVED FROM ITS ELECTRONIC ENERGY BAND
DIAGRAM (LEFT). ¹⁷ REPRINTED FROM PHYSICS REPORTS, 409, DRESSELHAUS, M.S., ET AL., 47-99, COPYRIGHT (2005),
FROM ELSEVIER 3
FIGURE 3. SCHEMATIC ILLUSTRATION OF THE COMPONENTS OF AN ATOMIC FORCE MICROSCOPE. 4813
FIGURE 4. PLOT OF ELECTRONIC TRANSITION ENERGIES (E _{II}) VS DIAMETER OF NANOTUBE (D _T). TREPRINTED FROM PHYSICS
REPORTS, 409, DRESSELHAUS, M.S., <i>ET AL.</i> , 47-99, COPYRIGHT (2005), FROM ELSEVIER17
FIGURE 5. REPRESENTATIVE RAMAN SPECTRUM OF HIPCO SWNTs FUNCTIONALIZED WITH GRAFT COPOLYMER ON A SILICON
SUBSTRATE (USING A 532 NM LASER EXCITATION WAVELENGTH). THE SPECTRUM HIGHLIGHTS REGIONS OF INTEREST: RBM
(PINK BOX), AND THE G-BAND (GREEN BOX)18
FIGURE 6. VARIOUS POLYMER ARCHITECTURES, INCLUDING LINEAR, CYCLIC, STAR AND BRANCHED20
FIGURE 7. (A) REPRESENTS A SIMPLE FLUID IN A "PANCAKE" CONFORMATION. (B) REPRESENTS A BOTTLEBRUSH POLYMER. 42
REPRINTED FROM PROGRESS IN POLYMER SCIENCE, 33, SHEIKO, S.S. ET AL., 759-785, COPYRIGHT (2008), WITH
PERMISSION FROM ELSEVIER21
FIGURE 8. SCHEMATIC REPRESENTATION OF DIFFERENT BBP CONFORMATIONS AS WELL AS CORRESPONDING AFM HEIGHT
MICROGRAPHS. ⁴² REPRINTED FROM PROGRESS IN POLYMER SCIENCE, 33, SHEIKO, S.S. <i>ET Al.</i> , 759-785, COPYRIGHT
(2008), WITH PERMISSION FROM ELSEVIER22
FIGURE 9. CONFORMATIONAL CHANGE FROM FLEXIBLE (A) TO ROD-LIKE IS INDUCED AS THE MOLECULAR WEIGHT OF SIDE CHAINS
is increased. ⁷⁶ Reprinted from Nature, 440, Sheiko, S.S., <i>et. al.</i> , 191-194, Copyright (2006), with permission
FROM Springer Nature23

FIGURE 10. ILLUSTRATION OF THE THREE METHODS FOR SYNTHESIS OF GRAFT POLYMERS: GRAFTING THROUGH, GRAFTING ONTO
GRAFTING FROM. ⁴² REPRINTED FROM PROGRESS IN POLYMER SCIENCE, 33, SHEIKO, S.S. <i>ET Al.</i> , 759-785, COPYRIGHT
(2008), WITH PERMISSION FROM ELSEVIER25
FIGURE 11. FTIR SPECTRA (A) OF PF-BR AND PF-N ₃ INDICATING THE APPEARANCE OF A SHARP STRETCH AT ~2090 CM
CORRESPONDING TO THE AZIDE GROUP (DOTTED LINE). FTIR SPECTRA NORMALIZED TO FIT IN THE 0-1% TRANSMITTANCE
RANGE. ¹ H NMR SPECTRA (B) OF PF-BR AND PF-N₃ SHOWING THE UPFIELD SHIFT OF PROTONS WITH THE SUBSTITUTION
TO THE AZIDE GROUPS. BOTH SPECTRA CALIBRATED TO THE RESIDUAL SOLVENT PEAK AT 7.26 PPM. INSETS SHOW A CLOSEF
LOOK AT THE PEAKS OF INTEREST30
FIGURE 12. FTIR SPECTRA OF ALL GRAFT COPOLYMERS AFTER SPAAC, INDICATING THE DISAPPEARANCE OF THE AZIDE STRETCH
at $\sim\!2090$ cm ⁻¹ (marked by the dotted line) after 5 minutes. Spectra normalized to fit in the 0-1%
TRANSMITTANCE RANGE33
FIGURE 13. ¹ H NMR SPECTRA OF GRAFT COPOLYMERS IN CDCL ₃ (CALIBRATED TO 7.26 PPM) INDICATING AN INCREASE IN
PROTONS ATTRIBUTED TO THE MPEG SIDE CHAINS32
FIGURE 14. THERMOGRAVIMETRIC ANALYSIS CURVES OF ALL GRAFT COPOLYMERS ALONG WITH BACKBONE POLYMER35
FIGURE 15. AFM IMAGES OF ALL FOUR GRAFT COPOLYMERS SHOWING A CONFORMATIONAL CHANGE AS THE SIDE CHAIN
increases in molecular weight. Samples of 20 or 40 μL (as labelled) were spin-cast onto silicon from μ
SOLUTION OF 2MG/2ML IN THF37
FIGURE 16. UV-VIS ABSORPTION SPECTRA OF GRAFT COPOLYMERS INDICATING THE ABSORBANCE OF PF-N ₃ IN EACH SAMPLE. 39
FIGURE 17. DISPERSIONS OF SWNTS USING GRAFT COPOLYMERS WITH INCREASING MOLECULAR WEIGHTS OF SIDE CHAINS (LEFT
to right: 5, 10, 20, 40 kDa) in Water (A) and THF (B)41
FIGURE 18. UV-VIS-NIR SPECTRA OF DISPERSIONS IN WATER (A) AND THE (B) USING GRAFT COPOLYMERS. ALL SPECTRA
NORMALIZED TO 380 NM42
FIGURE 19. FULL RAMAN SPECTRA OF DISPERSIONS USING ALL FOUR GRAFT COPOLYMERS IN THE AND WATER. SPECTRA WITH
λ_{EX} = 532 NM WAS NORMALIZED TO ~1586 CM ⁻¹ , WITH λ_{EX} = 633 WAS NORMALIZED TO ~1591 CM ⁻¹ AND WITH λ_{EX} = 735 WAS
NORMALIZED TO 1587 CM ⁻¹ . The peak at 520 cm ⁻¹ corresponds to the silicon substrate. 5543

List of Supporting Figures

FIGURE S1. ¹H NMR OF COMPOUND 1 IN CDCL3 (*) WHERE (~) REPRESENTS ETHANOL, (•) REPRESENTS WATER AND (×
REPRESENTS ACETONE
FIGURE S2. ¹H NMR OF COMPOUND 2 IN CDCL3 (*) WHERE (×) REPRESENTS ACETONE, (•) REPRESENTS WATER AND (◆
REPRESENTS METHANOL
FIGURE S3. ¹ H NMR of compound 3 in CDCL ₃ (*) where (•) represents water and (♦) represents methanol 6.
FIGURE S4. ¹H NMR of COMPOUND 4 IN CDCL3 (*) WHERE (•) REPRESENTS WATER AND (♦) REPRESENTS METHANOL 6
FIGURE S5. ¹H NMR of COMPOUND 5 IN CDCL3 (*) WHERE (•) REPRESENTS WATER, (⊗) SILICON GREASE AND (♦) REPRESENT
METHANOL
FIGURE S6. ¹H NMR OF COMPOUND 6 IN CDCL ₃ (*) WHERE (•) REPRESENTS WATER, AND (⊗) SILICON GREASE
FIGURE S7. ¹H NMR of Compound 8A (REPRESENTATIVE OF COMPOUNDS 8B-D) IN CDCL ₃ (*) WHERE (•) REPRESENTS WATER
(\varnothing) N-hydroxysuccinimide, (\land) represents diethyl ether and (\cap) represents hexanes. Inset shows the ful
SPECTRUM WITHOUT MAGNIFICATION
FIGURE S8. ¹ H NMR of Compound 9A (REPRESENTATIVE FOR COMPOUNDS 9B-D) IN CDCL ₃ (*). Inset shows spectrum
WITHOUT MAGNIFICATION
FIGURE S9. GPC TRACE OF POLY(FLUORENE) (PF-N3).
Figure S10. AFM images of PF-N $_3$ spin-cast onto silicon. Samples were prepared by spin-casting 20 μL of
2MG/2ML IN THF ONTO A SILICON SUBSTATE
FIGURE S11. PRELIMINARY AFM IMAGES OF GRAFT COPOLYMER WITH 40 KDA SIDE CHAINS. ALL IMAGES ARE ON SILICO
CLIPSTDATE ADDITIONAL SAMPLE PREDABATION INFORMATION OLITHINED LINDED EACH IMAGE

M.Sc	c. Thesis – Unnati Desai	<u> McMaster University – Chemistry a</u>	ınd Chemical Biology
Figur	E S12. AFM IMAGE OF 5 KDA DISPERSION	I SAMPLE IN THF SPIN CAST ONTO SILICON SUBST	RATE. THERE ARE NO SWNTS
	SEEN IN THIS IMAGE		69
Figur	E \$13. (A) SERIAL DILUTIONS OF PF-N ₃ IN	THF STARTING WITH A STOCK SOLUTION OF 1MG/1	0mL. 2mL of each solution
	was added for a total of 3mL volume	IN THE CUVETTE FOR UV-V IS MEASUREMENTS. (B) THE RESULTANT STANDARD
	CURVE WITH LINEAR TRENDLINE FROM THE	SERIAL DILUTIONS.	71

M.Sc. Thesis – Unnati Desai	McMaster University – Chemist	rv and Chemical Biology
	,,,,,,,,	,

List of Schemes

SCHEME 1. PREPARATION OF BACKBONE POLYMER, POLY(FLUORENE) WITH PENDENT AZIDE GROUPS (PF- N_3)	29
SCHEME 2. PREPARATION OF GRAFT CHAINS USING MPEG-AMINES OF MOLECULAR WEIGHTS 5 (8A), 10 (8B), 20 (8C), A	4ND 40
KDA (8D)	31
SCHEME 3. PREPARATION OF GRAFT COPOLYMERS (PF-G-MPFG) VIA STRAIN-PROMOTED AZIDE ALKYNE CYCLOADDITION	32

Chapter 1: Introduction

1.1 Single-Walled Carbon Nanotubes (SWNTs)

Since lijima's seminal images of carbon nanotubes (CNTs)¹, these nanomaterials have garnered significant scientific attention. CNTs may be visualized as layers of graphene rolled into a cylindrical tube.^{2,3} While CNTs are allotropes of carbon, like diamond, graphite and fullerene, they are distinguished by their cylindrical structure made up of sp² hybridized carbon atoms.⁴ As such, CNTs form a "hexagonal-shaped lattice" with π-bonds along the entire cylindrical tube.3 These materials are further categorized as single- (SWNTs) and multi-walled carbon nanotubes (MWNTs). SWNTs consist of a single graphene layer whereas MWNTs are made up of two or more layers.^{5,6} SWNT diameters are reported between 0.8-2 nm^{7,8} and lengths ranging from 10 nm to 1 cm.^{9,10} This means SWNTs have a high aspect ratio.¹¹ Beyond this, SWNTs are found in a mixture wherein they are varied in their diameters, helicities and presence of defects throughout the tube ends and sidewalls.⁷

1.2 SWNT Properties

Owing to their structure, SWNTs possess exceptional electrical, mechanical and thermal properties. 12 SWNT's electrical properties are dependent on the way in which the cylindrical tube is "rolled" or what is known as the roll-up vector, $C_h = na_1 + ma_2$ (Figure 1).7 By "rolling" a 2-D graphite sheet into a quasi-1D nanotube, van Hove singularities (VHS) (energy levels with high density of states (DOS)) are formed. As such, SWNTs can have semiconducting or metallic behaviour depending on the chirality and diameter of each nanotube. When n=m, the nanotube is referred to as "armchair," when m=0 it is called

"zigzag" and all other tubes are known as "chiral." Armchair tubes are all metallic whereas zigzag and chiral can be metallic if n-m=3l (where l is an integer) and semiconducting when $n-m\neq 3l$. Generally, it has been determined that one third of all CNTs are metallic and the remaining two thirds are semiconducting. 15,16

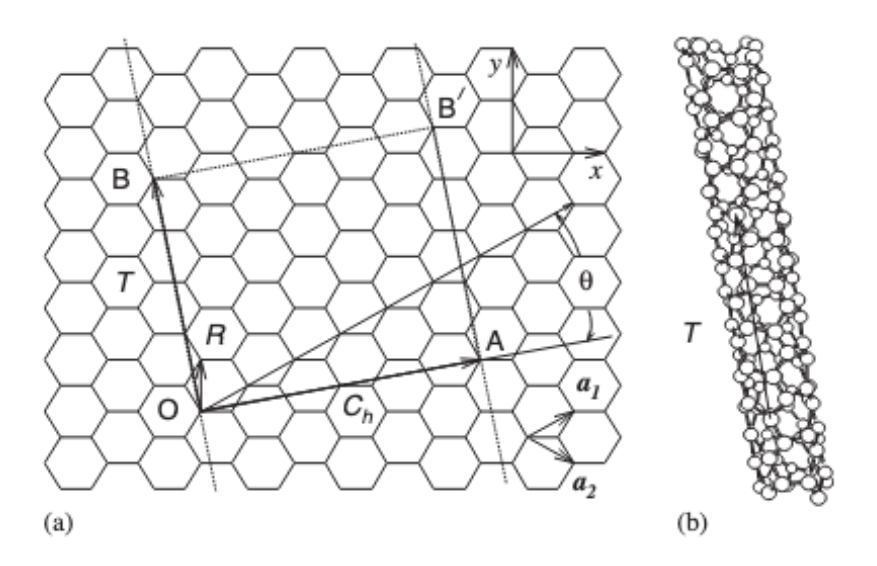


Figure 1. Schematic shows unrolled (a) and rolled (b) graphene sheet of a (4, 2) nanotube. Connection of sites O and A and B and B' result in the rolled sheet (b). Roll-up vector C_h is expressed by vector OA and translational vector T is expressed by vector OB.¹⁷ Reprinted from Physics Reports, 409, Dresselhaus, M.S., *et al.*, 47-99, Copyright (2005), with permission from Elsevier.

Because of the variation in nanotube circumference, band gaps of these tubes are wide-ranging with different allowed valence (highest occupied molecular orbital (HOMO)) and conduction (lowest unoccupied molecular orbital (LUMO)) states. The increase in diameter increases the number of allowed states and decreases the spacing between each state. This means nanotubes can have a zero band gap (like metals) or band gaps that span

the range of 0.5-1 eV¹⁸ based entirely on the diameter of individual tubes.¹⁵ Because all armchair nanotubes are metallic, they are gap-less while non-armchair tubes are considered narrow-gap semiconductors (**Figure 2**).¹⁸

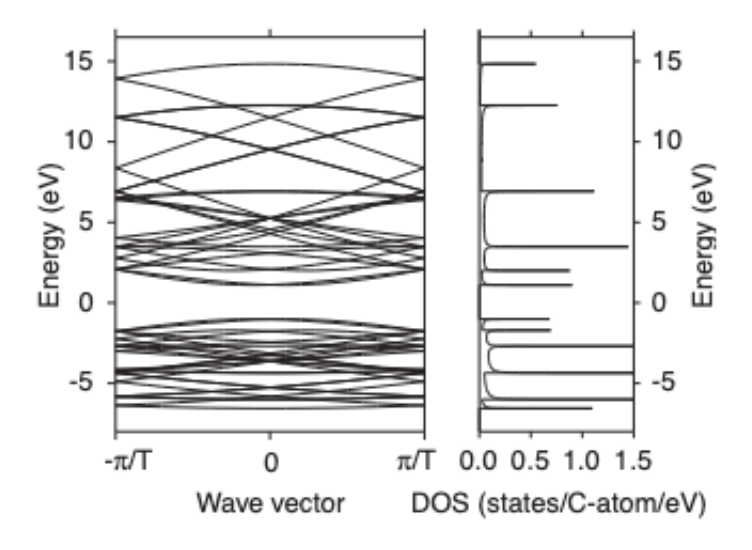


Figure 2. Illustration of the density of states (right) of a (4, 20) nanotube derived from its electronic energy band diagram (left).¹⁷ Reprinted from Physics Reports, 409, Dresselhaus, M.S., *et al.*, 47-99, Copyright (2005), with permission from Elsevier.

In addition to the notable electronic properties, CNTs have mechanical properties that are comparable to steel and Kevlar. Their Young's modulus has been reported to be 1.4 TPa with a tensile strength of 100 GPa which is beyond that of steel (Young's modulus of 200 GPa and tensile strength of 1-2 GPa). Furthermore, molecular dynamics simulations of CNTs wherein nanotubes were studied for axial compression, bending and torsion showed that CNTs can reversibly switch into different morphological patterns. It was found that CNTs

were able to reversibly bend at angles up to 110°.4 Ultimately, the simulations concluded the decidedly highly elastic nature of these nanomaterials.²⁰

Finally, CNTs also have a thermal stability of up to 2800°C in vacuum, thermal conductivity two times that of diamond and capability of carrying electric current 1000 times that of copper wires.⁴ In addition to these properties, owing to their chemically inert nature, particularly in the absence of defects, CNTs can also be useful for biological applications.¹⁹

1.3 Synthesis of SWNTs

While there are several methods for synthesis of CNTs, three main methods include: arc-discharge, laser ablation and chemical vapor deposition.²¹

1.3.1 Arc-Discharge

lijima and coworkers were the first to perform large-scale synthesis of CNTs using the arc-discharge method.²² This method uses an anode and a cathode, made of graphite, that are brought in close proximity under a pressurized atmosphere (helium or argon and methane) as a voltage is introduced.^{4,23} The chamber, which also contains evaporated carbon molecules along with metal catalyst particles, is heated to ~4000 K.¹³ During this process, the anode is consumed while the cathode develops solidified carbon on its surface, known as 'cylindrical hard deposit' or 'cigar-like structure.'¹³ At its core, the cathode also contains a "softer, fibrous" material which includes nanotubes along with other carbon particles.⁴ Arc-discharge produces SWNTs with an average diameter of 1.4 nm (and a range of 0.7 – 1.65 nm).^{13,23}

1.3.2 Laser Ablation

Laser ablation was first used by Smalley and co-workers in 1996 to produce high-yielding SWNTs.¹⁶ This process occurs in a reactor which contains a furnace and a water-cooled collector. First, a pulsed laser strikes at and vaporizes graphite at 1200°C in the presence of an inert gas (i.e. helium) and small amounts of Ni and Co.²³

Then, a second pulse is transmitted for a faster vaporization of the target graphite. As the vaporized carbon condenses, nanotubes begin to develop on the water-cooled surface of the reactor on catalyst atoms. The growth of the nanotubes continues until catalyst atoms begin to aggregate on the ends of the nanotubes. Laser ablation produces nanotubes that are 10-20 nm in diameter and hundreds of microns in length. Variation in temperature and catalyst among other parameters can alter the average diameter and length of nanotubes synthesized.²³

1.3.3 Chemical Vapour Deposition (CVD)

Chemical Vapour Deposition (CVD) works by growing SWNTs on the surface of a substate using catalyst nanoparticles as "seeds" for nanotube growth.^{2,21} The growth of the nanotubes is controlled by hydrocarbon carrier gas, growth time and temperature, and the catalyst. The choice of substrate also plays a major role in the types of nanotubes that are synthesized using this method.²³ The choice of substrates includes silicon, glass and alumina and the catalysts that can be used include metal nanoparticles made of Fe, Co or Ni. CVD uses a substrate, which contains catalyst particles, in a furnace at temperatures >800°C under atmospheric pressures.^{2,23} Once in the furnace, a hydrocarbon gas and a

M.Sc. Thesis – Unnati Desai McMaster University – Chemistry and Chemical Biology process gas (ammonia, nitrogen, hydrogen) is supplied and reacted.^{2,23} Upon decomposition of the hydrocarbon gas, nanotubes are formed on the catalyst.²³ This type of synthetic method generates SWNTs that are long, ranging up to hundreds of microns.² The diameter of

the nanotubes synthesized depends on the particle size of the chosen catalyst.²³

1.3.4 Variations of CVD

There are several variations of the CVD method; namely some of these include plasma enhanced CVD (PECVD), high pressure Carbon Monoxide disproportionation (HiPCo) and the CoMoCAT process.

The PECVD method is able to synthesize nanotubes that are well-aligned and straight. In this method a substrate is coated with a Ni catalyst and introduced to high purity ammonia as the catalytic gas and acetylene as the carbon source. Plasma is generated using a direct-current while a carbonized tungsten filament provides heat as well as aids in the dissociation of the gases. As growth time and temperature are varied, the nanotube length is also altered. Nanotubes prepared by this method grow in the direction of the plasma that is generated.⁴

The high pressure carbon monoxide disproportionation (HiPCo) process produces nanotubes that are high in purity²⁴ and are commonly reported in literature for SWNT research applications. This method uses a catalyst in the gas phase.²³ Iron pentacarbonyl (Fe(CO)₅) and CO gas are injected at the same time at high pressure and temperature. The iron, in the form of metal clusters, acts as the catalytic site. When the metal clusters adopt the size of C_{60} they begin to nucleate and form SWNTs. The SWNTs are believed to continue

to grow until the metal cluster reaches a size that forms a carbon shell around the cluster. HiPCo nanotubes have an average diameter of 1.1 nm (with ranges of 0.7-1.2 nm²⁵).²⁴

Finally, the CoMoCAT process makes use of cobalt and molybdenum as catalysts for nanotube synthesis. In this process, SWNT synthesis occurs by the decomposition of carbon and CO_2 using a CoMo catalyst at 700-950°C. Pure CO flows at a pressure between 1-10 atm resulting in SWNT growth in just a few hours.²³ This process generates SWNTs with diameters of ~0.8 nm.²⁵

1.4 Functionalization of SWNTs

Despite their inherent exceptional properties and regardless of the synthetic method used, CNT application is stunted because of self-aggregation of individual nanotubes. It has been demonstrated that CNT samples form bundles of 20-100 individual nanotubes. Strong van der Waals attraction between CNTs prevents their dispersion in aqueous and organic media. Bundling of nanotubes also disrupts their electronic structure and prevents the separation of nanotubes by size or type. As a solution, functionalization of CNTs has become a major area of scientific research. Functionalization of CNTs allows for improved solubility and processibility and the transfer of the properties of various functionalities onto nanotubes. Through the introduction of functional groups to CNTs, aggregation is prevented; it provides a barrier between individual nanotubes thereby reducing van der Waals attraction. Beyond preventing self-aggregation, functionalization offers CNTs with additional advantages: reactivity and solution processibility are improved and further modification is achieved depending on the type of functionalization used.

Generally, there are two approaches to CNT functionalization: endohedral and exohedral. Endohedral functionalization involves the modification of CNTs on the inside and includes methods such as metal encapsulation (encapsulation of metals such as Fe, Co, Ni, Ti and Cu) and fullerene encapsulation (encapsulation of C_{60} , C_{70} or metalofullerenes). Exohedral functionalization works by introducing functional groups to the outside of CNTs. This type of functionalization is subdivided as covalent or non-covalent exohedral functionalization.

1.4.1 Covalent Functionalization

Earliest covalent functionalization of SWNTs involved treatment of nanotubes with mixtures of acids (i.e. sulfuric, nitric, piranha, etc.) or ozone at high temperatures in order to rid raw nanotubes of impurities (metal catalyst particles) and to "cut" or "etch" them in a technique termed "oxidative purification." This etching/cutting introduces oxygenated functionalities to the ends of the nanotubes. Thus, the ends are left open with some number of carboxylic acid, anhydride, quinone and/or ester functionalities attached. It is understood these functionalities are most concentrated on the ends of the nanotubes but can also be sporadically found along the rest of the nanotube where curvature strain is increased resulting in amplified reactivity. Therefore, covalent functionalization can be performed on the termini of the tubes or on the sidewalls. Further functionalization of the introduced carboxylic and hydroxyl groups can be attained; from carboxylic acids, carboxamides can be prepared and subsequent attachment of aliphatic and aryl amines, amino acid derivatives and peptides can be achieved. Regardless of the type of functionality, these are effective functionalizations as they can lead to dispersions of CNTs in water and organic media as

M.Sc. Thesis – Unnati Desai McMaster University – Chemistry and Chemical Biology well as lead to enhanced hydrophilicity, granting CNTs increased biocompatibility and biodegradability. However, one major disadvantage of this type of functionalization is that it introduces defects along the CNT sidewall, leading to disruption in the π -conjugation and deleterious impact on nanotube properties.¹⁹

1.4.2 Non-Covalent Functionalization

In contrast to covalent functionalization, non-covalent functionalization retains the intrinsic CNT properties by maintaining the π -conjugation of the tube. This type of functionalization is driven by strong π - π , CH- π , NH- π or hydrophobic interactions. This is done by first agitating (generally via sonication) some type of dispersant in the presence of SWNTs. Dispersants may be a surfactant, a biomolecule, aromatic molecules or polymers.

When a surfactant is used, the hydrophobic nature of the molecule interacts with the surface of the CNT sidewalls and organizes such that the hydrophilic head points toward the water. Some surfactants used for CNT dispersions include sodium dodecyl sulfate (SDS), sodium dodecyl benzene sulfonate (SDBS), sodium cholate (SC), cethyltrimethylammonium bromide (CTAB), Brif, Tween, and Triton X.²⁹ DNA can also be used, with its nucleobases forming π - π stacking interactions with the π -surface of the CNT. DNA is able to helically wrap around the CNT surface and successfully disperse CNTs in water.²⁵ DNA wrapping of nanotubes not only disperses CNTs but also allows for selectivity of a narrow range of nanotube diameters.31

In the case of aromatic molecules, similar to DNA, π -stacking interactions between the aromatic structure and the nanotube surface are formed. Unlike a graphene sheet, CNTs have a curvature to their structure. As a result, there is a misalignment of the π -orbitals such that adjacent carbon orbitals have a misalignment angle (ϕ) between them. This structurally manifests as pyramidalization of carbon atoms due to strain in nanotube sidewalls. It is understood that the diameter of a CNT is indirectly proportional to the pyramidalization angle and the π -orbital misalignment angle. Through the DFT (density functional theory) calculations performed by Tournus and Charlier, studying adsorption of benzene on chiral and armchair SWNTs, it was demonstrated that benzene had the strongest adsorption where π -orbital misalignment was minimal. This showed that wider nanotubes had a higher binding energy for benzene and that interactions of molecules with SWNTs are dependent on the nanotube curvature as well as the orbital orientation.

The use of polymers, and specifically conjugated polymers, is arguably one of the most studied techniques for functionalization of CNTs. The driving force of these dispersions is the π - π interaction of the long conjugated backbone of the polymer with the π -surface of the CNT. This interaction allows the debundling of CNTs and improves their dispersibility. Additionally, the use of conjugated polymers affords nanotubes with high selectivity and separation yield as well as the potential for large-scale processibility. Conjugated polymer-CNT complexes have been applied in a myriad of aspects including energy storage, electronic and optoelectronic devices and sensors, to name a few.

It was in 2007 that Nicholas and coworkers first used commercially-purchased conjugated polymers, such as poly(9,9-di-n-octylfluorene) to disperse semiconducting

SWNTs. Some examples include poly(*p*-phenylenevinylene) derivatives, pol(fluorene) derivatives, poly(3-alkylthiophenes), poly(pyrrole), and poly(aniline).¹² It's evident that the strategic design of polymers can provide different advantages to CNTs; from increased solubility to increased selectivity and biocompatibility; these are all possibilities for CNT dispersions using polymers. Consequently, countless numbers of polymers can be and have been synthesized in achieving these desired properties.

1.4.3 Aqueous Dispersions of SWNTs

One such desired property is the dispersion of CNTs in aqueous media. This is important because of the possibility for biological applications. It has been shown that aqueous dispersions of CNTs can be prepared using a variety of polymers and small molecules, including poly(vinylpyrrolidone), polystyrene sulfonate, poly(L-lysine)³⁸), crown ethers, glucosamines, DNA, peptides, proteins, surfactants, and starch.³⁹ Previously within the Adronov Group, conjugated graft copolymers were synthesized for aqueous SWNT dispersions.^{40,41} It was demonstrated that poly(fluorene)-*g*-poly(ethylene glycol monomethyl ether) (mPEG) polymers of increasing molecular weight (mPEG side chains of M_n 2, 5, 23.5, and 41 kDa) were able to disperse SWNTs in water using non-covalent interactions.⁴⁰ These were promising results for further exploration of advanced polymer architecture and its role in the dispersion and modification of SWNTs.

1.5 Characterization Techniques

To characterize polymers, techniques such as gel permeation chromatography (GPC), light scattering and viscometry are typically used. Yet these techniques fall short for the study of complex macromolecules like graft copolymers. For this reason, visualization of these macromolecules can serve as a powerful alternative.⁴²

To study nanotube properties, including morphological, structural and electronic, several characterization techniques can be employed;⁴³ some of these include UV-Vis-NIR spectroscopy (UV-Vis-NIR), Resonance Raman Spectroscopy (RRS) and Atomic Force Microscopy (AFM). Spectroscopy methods, like UV-Vis-NIR and Raman, measure nanotube dispersion properties through a light source and relate the absorbed or scattered light with particle size. Microscopy techniques allow for direct measurement of nanotube diameters and lengths.44

1.5.1 Atomic Force Microscopy (AFM)

The Atomic Force Microscope was introduced by Binning et al. in 1986. 45 This type of scanning probe microscope instrument includes a cantilever (with a sharp tip), a detector which monitors the cantilever's movement (typically a photodetector), a force transducer, a translation system (e.g. piezo tubes) in relation to the cantilever, and finally software that converts scans into a topographical map. 46

AFM works by scanning the surface of a sample using a sharp tip attached to the cantilever and utilizing the interactive force between the surface of a sample and the tip of the cantilever.⁴⁶ There are generally two modes for surface imaging of a sample; in the

M.Sc. Thesis – Unnati Desai

continuous contact mode, the cantilever tip is constantly touching the sample as the imaging is taking place while in the tapping mode there is intermittent contact with the sample. 46,47 The sharp tip is placed at the end of the cantilever where a laser beam is focused (**Figure 3**). The bending of the cantilever (contact mode) or the dampening of its oscillation amplitude (tapping mode) are monitored by the reflection of the laser beam onto a quadrant photodetector. When the interacting force between the sample and the tip is altered, the cantilever bends, which subsequently changes the location of the laser on the photodetector. 46 The photodetector can identify bending deflection, bending oscillation and torsion of the cantilever. 47

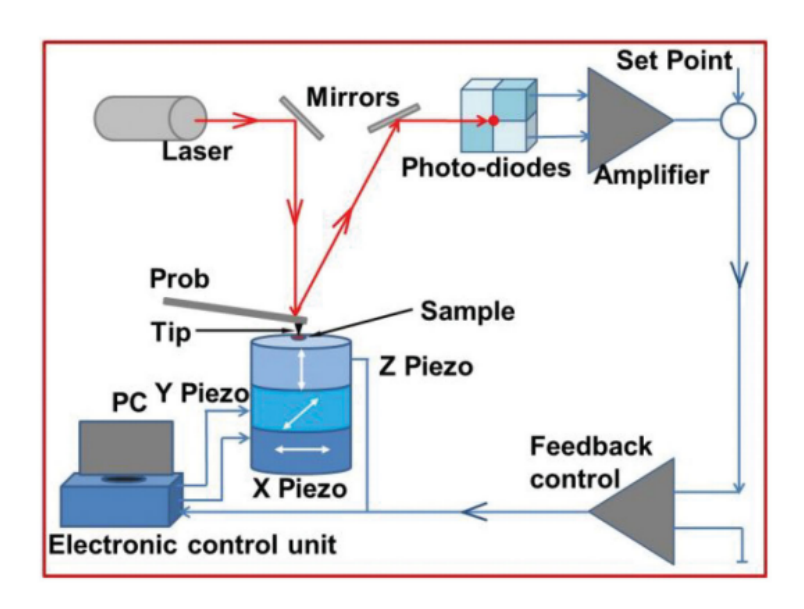


Figure 3. Schematic illustration of the components of an atomic force microscope.⁴⁸

Within the contact mode, a sample can be analyzed using constant force (the most common mode⁴⁷) wherein a continuous force is applied to the surface until a pre-set deflection takes place.⁴⁶ In this mode, the deflection point is kept constant while tracking

features of the sample.⁴⁷ Alternatively, constant height mode can be utilized. This mode is typically used for flat surfaces as it keeps the scanner height constant and the cantilever deflection is varied.⁴⁶ Contact mode is a fast, high-resolution imaging method. However, this mode may be detrimental for soft samples owing to the constant force being applied throughout the imaging process. This can result in damage to or loss of the sample and unclear imaging.⁴⁶

Oscillating mode, also called dynamic operation mode, is another route for AFM imaging of samples. In this mode the tip is only intermittently in contact with the surface of the sample, there is no vertical force, and lateral movement mostly occurs while the tip is not in contact with the surface (thereby reducing any lateral force). This is considered a milder approach to imaging than contact mode. It can be further classified into subcategories based on the value of amplitude used. Finally, jumping mode, also known as Quantitative Imaging mode or peak force mode is an additional option. This mode outputs a force-distance curve on each position of the sample and provides a topographical map as well as quantitative mechanical information.⁴⁶

AFM has been used in various ways to visualize polymers and CNTs as well as CNT-polymer composites for a myriad of reasons. Some examples of visualizations include AFM studies to identify patterns on DNA-wrapped CNTs⁴⁹, AFM visualization to measure molecular weight of polymers⁵⁰, AFM visualization to understand polymer architectures^{51–54} and AFM imaging to visualize dispersions and measure height profiles of polymer-wrapped CNTs.^{55–58}

1.5.2 UV-Vis-NIR Spectroscopy

UV-Vis-NIR spectroscopy is employed for examination of concentration, purity and chirality of SWNT samples. 43 Resulting from the quasi-1D structure of SWNTs, their absorption spectrum includes sharp peaks relating to the optical transitions of van Hove singularities (VHS) in the density of states (DOS).⁴³ The optical properties derived from these spectra are dependent on the structure of the SWNTs which is in turn dependent on the chiral vector (n,m) and diameter. ^{27,43} Different chiral vectors have different sets of inter-band transitions between VHSs, termed E₁₁, E₂₂, or S₁₁, S₂₂, etc.^{27,43,59} Semi-conducting SWNTs (sc-SWNTs) have four transition peaks on the UV-Vis-NIR spectrum: S₁₁, S₂₂, S₃₃, and S₄₄. The S₃₃ and S₄₄ transition regions overlap and are therefore considered to be one region. The lowest transitions are less spectrally overlapped and are the ones used for UV-Vis-NIR characterization purposes.⁵⁹ Metallic SWNTs (m-SWNTs) have only one transition: M₁₁ and all other transitions are outside the UV-Vis-NIR region.⁴³ On a spectrum, the electronic transitions of valence (v) to conduction (c) bands are signified by $vn \rightarrow cn$ where n is the band index. Wavelengths from 440-645 nm denote the v1 \rightarrow c1 ((lowest energy VHS) transitions (M₁₁)) accounting for metallic and semimetallic nanotubes. Wavelengths from 600-800 nm denote the v2 \rightarrow c2 transition (S₂₂) and 800-1600 nm denote the v1 \rightarrow c1 transition (S₁₁) of semi-conducting nanotubes. 60 Ultimately peaks in these wavelength ranges can determine purity of sample by identifying the presence of semiconducting and/or metallic nanotubes. Additionally, the disparity in intensities of different peaks comes from the difference in the abundance and absorption of individual nanotubes. 43

1.5.3 Resonance Raman Spectroscopy (RRS)

Raman spectroscopy measures the vibrational modes of molecules and is often used to provide them with a fingerprint.⁶¹ When light hits matter, it can exchange energy and momentum which leaves the matter changed. These changes can be seen as electronic excitation and/or molecular or rotational vibration. When a photon interacts with a molecule, it can experience elastic or inelastic scattering.⁶² Raman spectroscopy uses Raman scattering, otherwise known as inelastic photon scattering.⁶¹ The difference between elastic (Rayleigh scattering) and inelastic photon scattering is that elastic scattering does not result in energy transfer between the incident photon and the scattering materials, while inelastic scattering involves a difference in energy between the incident and scattered photon.⁶² Inelastic scattering results in a molecule that is in a modified vibrational state, generating a phonon (a quasi-particle), and is the basis for Raman spectroscopy.⁶² There are many types of Raman spectroscopy; some of these include surface-enhanced, resonance, tip-enhanced, polarized, Coherent, transmission, spatially offset and hyper Raman.⁶¹

Resonance Raman spectroscopy (RRS) is the most commonly used method to characterize individual SWNTs by identifying their chiralities. ^{18,43} It provides information on SWNT diameter as well as purity (whether the sample is semi-conducting or metallic) and can be used for analyzing bundles and sorted CNTs. ^{63,64} As previously discussed, the chiral vector determines the electronic nature of SWNTs and the quasi-1D nature of nanotubes forms VHSs. Upon excitation of a laser with a specific wavelength, the energy of the laser can be equal to or different from the transition energy of the valence and conduction bands of the VHSs. When this energy is equal, a Raman signal is produced. ⁶⁴ Therefore, to

M.Sc. Thesis – Unnati Desai

characterize CNTs using Raman, the plot of energy (E_{ii}) vs. nanotube diameter is important (**Figure 4**).⁶⁴ The points on the graph represent the optical energy of a given nanotube (n, m). Based on the energy of the laser used, specific nanotubes will be observable, as outlined by **Figure 4**.⁶⁴ For this reason, to get a comprehensive idea of the types of nanotubes in a sample, multiple lasers are required for analysis.

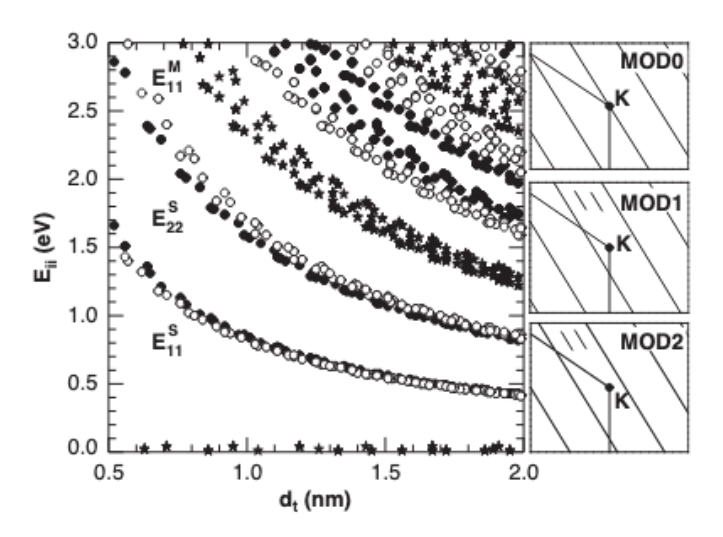


Figure 4. Plot of electronic transition energies (E_{ii}) vs diameter of nanotube (d_t).¹⁷ Reprinted from Physics Reports, 409, Dresselhaus, M.S., *et al.*, 47-99, Copyright (2005), with permission from Elsevier.

Four main regions make up a Raman spectrum: the radial breathing mode (RBM) (~100-400 cm⁻¹), the D-band (~1250-1450 cm⁻¹), the G-band (~1550-1595 cm⁻¹) and the G'-band (~2500-2900 cm⁻¹).⁶⁵ The main features used to characterize SWNTs are the tangential mode (G band) and the radial breathing mode (RBM) (**Figure 5**).^{43,66}

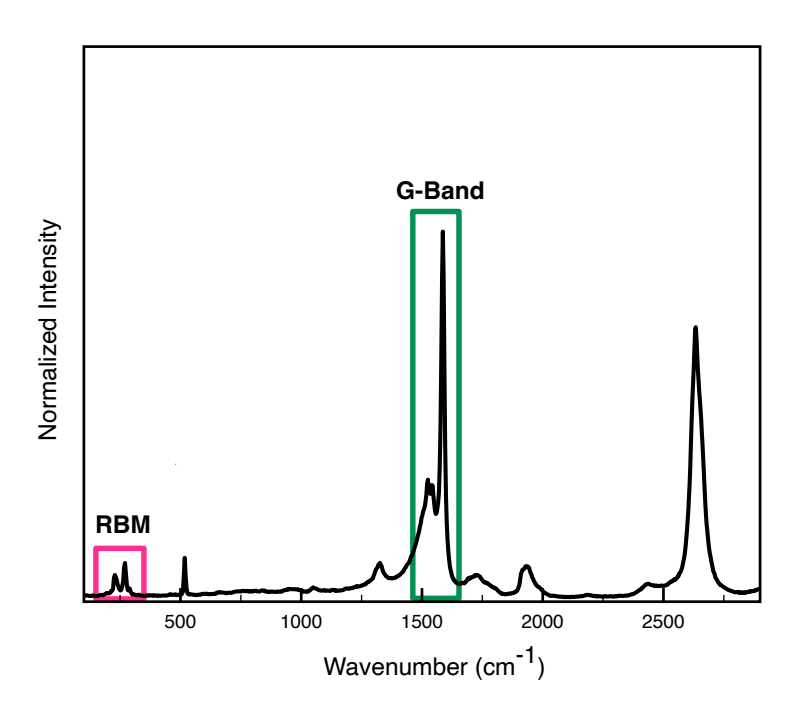


Figure 5. Representative Raman spectrum of HiPCo SWNTs functionalized with graft copolymer on a silicon substrate (using a 532 nm laser excitation wavelength). The spectrum highlights regions of interest: RBM (pink box), and the G-Band (green box).

The RBM is a vibrational mode in which the nanotube's carbon atoms move symmetrically in a radial direction, expanding and contracting the tube's circumference. RBM is determined by the nanotube diameter, as seen in eq. 2 where ω is the vibration frequency, A and B are constants and d_t is the diameter of the nanotube. 67

$$\omega_{RBM} = \frac{A}{d_t} = B \tag{eq. 2}$$

As the equation states, the vibration frequency is inversely related to the diameter of the nanotube.⁶⁸ Conveniently, at a particular excitation energy, the metallic and semi-

M.Sc. Thesis – Unnati Desai McMaster University – Chemistry and Chemical Biology conducting nanotubes that are in resonance have significantly different diameters (**Figure**4), allowing them to be distinguished through analysis of peaks in the RBM region.

The tangential mode or G band has a distinctive line shape depending on the metallic or semiconducting nature of the nanotube.⁶⁷ It splits into two peaks termed G⁻ and G⁺ peaks.⁴³ The G⁺ represents the displacements along the axis of the tube and G⁻ represents the displacements around the circumference of the axis.⁶⁴ The lineshape of the G⁻ band is broad for m-SWNTs and has a Lorentzian shape for sc-SWNTs. Using the energy vs diameter plot (**Figure 4**), the diameter ranges for sc- and m-SWNTs can be predicted.⁶⁴

1.5.4 Thermogravimetric Analysis (TGA)

Thermogravimetric analysis is used to measure the mass loss of a sample as it is gradually heated to high temperatures. The sample can be heated at a constant rate (dynamic measurement) or kept static at one temperature (isothermal measurement). The atmosphere under which samples are varied can be reactive, oxidising or inert. TGA results are depicted as a plot of mass or percent mass loss vs. temperature or time. A mass loss event is seen on a curve as a step and occurs when the sample loses material through evaporation, oxidation, oxidative decomposition, thermal decomposition, or loss of water.⁶⁹

1.6 Graft Copolymers

Polymer architecture, including linear, cyclic, star and branched (**Figure 6**), is a fundamental characteristic in determining the bulk (e.g. rheological, mechanical) and solution (shear viscosity, self-assembly) properties of polymers.

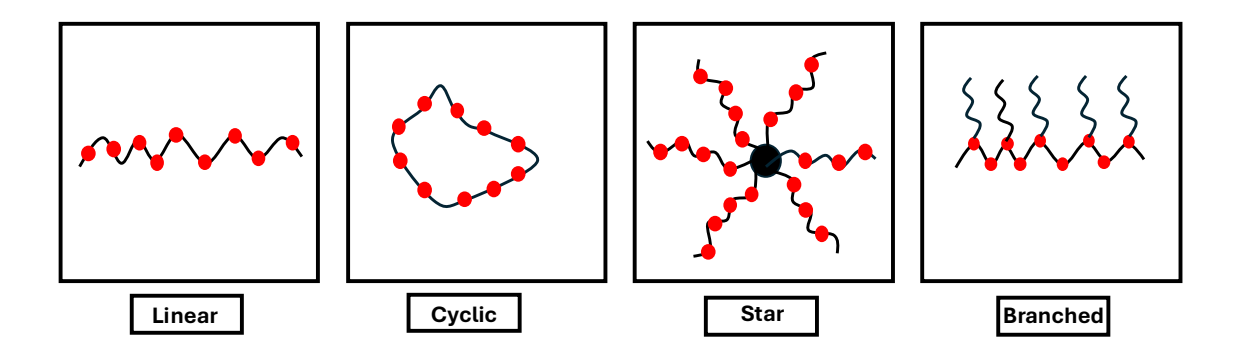


Figure 6. Various polymer architectures, including linear, cyclic, star and branched.

Owing to their architecture, graft copolymers in particular have potential for a myriad of applications; this includes lithographic photoresists, bio-lubrication, nanomedicines, super-soft elastomers, drug delivery agents, molecular sensors, self-assembling materials, thermoplastics, photonic crystals, ion transport, and energy storage.^{70,71}

Graft copolymers (molecular combs and bottlebrushes) are linear chain backbones with side chains grafted onto them. These are markedly different from their linear analogues. Three parameters define graft polymers: the degree of polymerization of the backbone and side chains, the grafting density of the side chains, and the spacer between two neighbouring side chains. 70,72

1.6.1 Bottlebrush Polymers (BBPs)

Bottlebrush polymers (BBPs) are a sub-class of graft copolymers wherein a polymer backbone contains densely grafted short polymeric side chains (typically this translates to one side chain per backbone repeat unit⁷³).^{74,75} The addition of densely grafted side chains induces a cylindrical conformation in BBPs. This conformation is a result of two opposing

forces; the grafted chains repel each other but their movement away from each other is restricted by their covalent attachment to the backbone. Interestingly, because of this grafted chain repulsion, BBP backbones can coil in certain sections of the chain while maintaining a cylindrical shape.⁴² Additionally, owing to the circular distribution of side chains and the stretched conformation of the backbone, BBPs can form unique morphologies distinctly different from linear polymers that have the same functionality as the side chains.⁴²

Whereas simple fluids can adopt various shapes when adsorbed to a surface, the shapes of BBPs are restricted by their architecture.⁴² When a BBP adsorbs on a surface, its cylindrical symmetry is disrupted. The result is segmentation of its side chains.

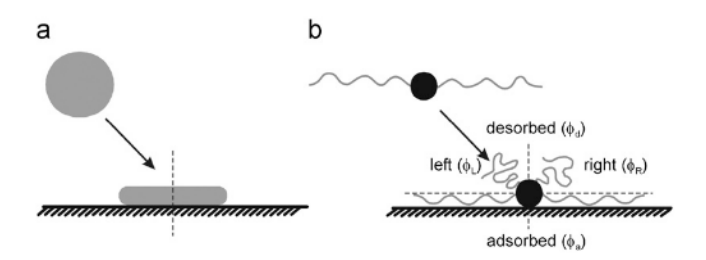


Figure 7. (a) represents a simple fluid in a "pancake" conformation. (b) represents a bottlebrush polymer.⁴² Reprinted from Progress in Polymer Science, 33, Sheiko, S.S. *et al.*, 759-785, Copyright (2008), with permission from Elsevier.

The kinds of shapes or conformations a BBP adopts when it adsorbs on a surface is determined by the portion of side chains that adsorb to the surface and the asymmetrical distribution of side chains on the backbone. When the number of adsorbed side chains/total

number of side chains (φ_a) is \cong 1 and chains adsorbed on the right (φ_R) \cong chains adsorbed on the left $(\varphi_L) = 0.5$, the brush adopts an extended ribbon-like conformation (**Figure 8**(b)).

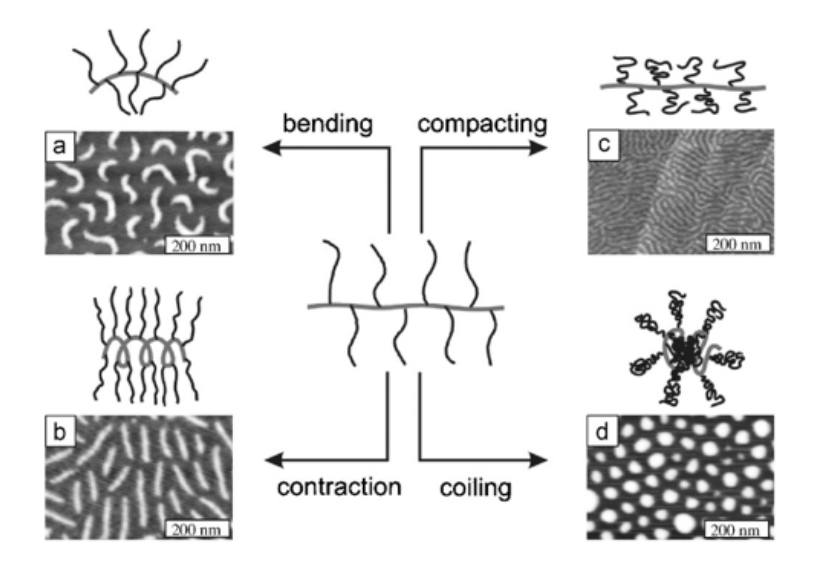
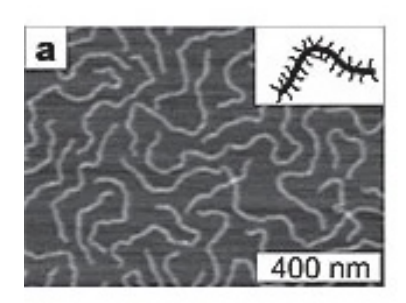


Figure 8. Schematic representation of different BBP conformations as well as corresponding AFM height micrographs.⁴² Reprinted from Progress in Polymer Science, 33, Sheiko, S.S. *et al.*, 759-785, Copyright (2008), with permission from Elsevier.

This is considered energetically favourable because most of the polymer is in contact with the surface. When φ_a < 1, the BBP side chains are no longer strongly adsorbed on the surface, and several different conformations are adopted depending on the environment of the BBP. When φ_a < 1, $\varphi_R \cong \varphi_L = 0.5$ and with repulsion between the desorbed side chains, a cylindrical conformation is observed (**Figure 8**(c)). When φ_a < 1, $\varphi_R \cong \varphi_L = 0.5$ and there is attraction between the desorbed side chains, a globular conformation (**Figure 8** (d)) is seen. Finally, when $\varphi_R \neq \varphi_L$ BBPs develop a spontaneous curvature as seen in **Figure 8** (a).⁴²



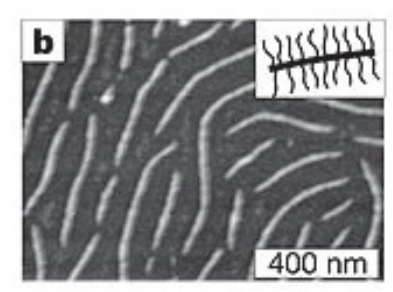


Figure 9. Conformational change from flexible (a) to rod-like is induced as the molecular weight of side chains is increased.⁷⁶ Reprinted from Nature, 440, Sheiko, S.S., *et. al.*, 191-194, Copyright (2006), with permission from Springer Nature.

Furthermore, the degree of polymerization of side chains (or in other words the molecular weight of side chains) can also play a role in conformations of BBPs observed. **Figure 9** shows AFM images of BBPs with backbones made up of poly(2-hydroxyethyl methacrylate) and side chains of poly(n-butyl acrylate) (pBA). The degree of polymerization of the backbone is consistent between the two images. However, a series of side chains were synthesized with the degree of polymerization ranging from $n = 12 \pm 1$ to $n = 140 \pm 12$. **Figure 9** (a) shows BBP with side chains where n = 12 and **Figure 9** (b) shows BBP with side chains where n = 130. As the degree of polymerization of side chains is increased, the BBP experiences a conformational change from a flexible curved (**Figure 9**(a)) conformation to a more rigid, rod-like conformation (**Figure 9**(b)).^{42,76}

1.6.2 Comb vs Bottlebrush Polymers

The distinction between a comb polymer and bottlebrush polymer is made through the degree of polymerization of the side chains ($N_{\rm sc}$) and their grafting density, z.⁷⁷ In fact, four conformations have been identified: loosely grafted comb, densely grafted comb,

M.Sc. Thesis – Unnati Desai McMaster University – Chemistry and Chemical Biology

loosely grafted bottlebrush, and densely grafted bottlebrush. Polymers are considered loosely grafted combs when the spacers between side chains are longer than the side chains $(z < 1/N_{sc})$ and densely grafted when the spacers are shorter than the side chains $(1/N_{sc} < z < z^*)$ where z^* is represented by equation 1 and b represents the Kuhn length (refers to the relative flexibility of the backbone⁷⁹); l represents the monomer length and v represents the monomer volume.

$$z^* \approx \frac{(bl)^{\frac{3}{2}}}{v} N_{sc}^{-1/2}$$
 (eq. 1)

When $z \approx z^*$, a loosely grafted bottlebrush conformation is achieved while $z > z^*$ results in a true, densely grafted bottlebrush polymer. At the point between loosely and densely grafted bottlebrush polymers, side chains begin to adopt an extended conformation. This conformation is seen if the spacer between neighbouring side chains starts to extend or if the entire backbone approaches an extended conformation.⁷⁷

1.7 Graft Copolymer Synthesis

To synthesize graft copolymers, there are three main approaches: "grafting through", "grafting onto" and "grafting from" (**Figure 10**)⁴² These synthetic techniques can be used alone or in combination with one another.⁷⁰

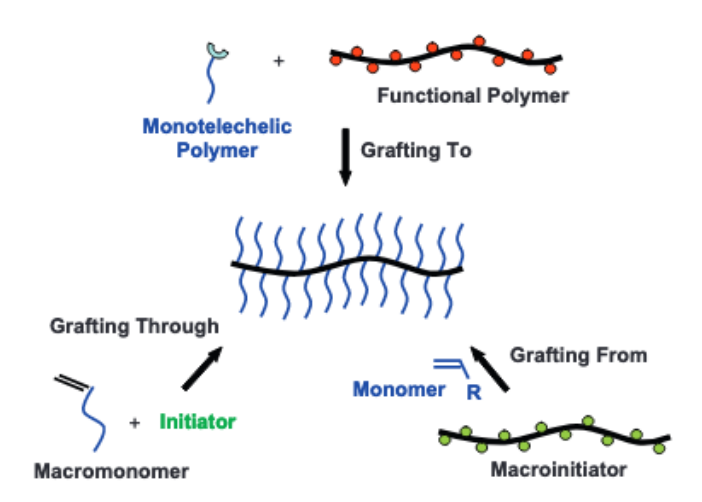


Figure 10. Illustration of the three methods for synthesis of graft polymers: grafting through, grafting onto, grafting from.⁴² Reprinted from Progress in Polymer Science, 33, Sheiko, S.S. *et al.*, 759-785, Copyright (2008), with permission from Elsevier.

1.7.1 Grafting-through Method

In the grafting-through method, graft polymers are synthesized using macromonomers creating polymers denoted polymacromonomers.⁸⁰ These macromonomers are polymerized to form the desired graft polymer.⁷⁰ The types of polymerizations used with this method are anionic, ring-opening metathesis and free radical polymerizations. A key advantage of this method is that it ensures there is a graft chain on every repeat unit.⁸⁰ On the contrary, this technique may provide low molecular weights of polymer if the macromonomer conversion is low.⁷⁰

1.7.2 Grafting-to Method

The grafting-to method requires separate synthesis of side chains and backbone polymer. Side chains are end-functionalized to be complementary with reactive monomer

M.Sc. Thesis – Unnati Desai McMaster University – Chemistry and Chemical Biology units on the linear backbone polymer. The coupling of the two complementary units results in the final graft polymer. This type of grafting technique uses click reactions such as coppercatalyzed azide-alkyne 1,3-dipolar cycloaddition and thiol-ene coupling reactions. One disadvantage of this method is the potential hindrance in synthesizing high-density grafted polymers. As more side chains are grafted onto the backbone, the steric repulsion between the side chains increases. This repulsion could potentially prevent additional side chains

1.7.3 Grafting-from Method

from being grafted onto the backbone.70

The grafting-from method uses a macroinitiator with some number of initiation sites pre-installed on the backbone polymer. Polymerization occurs directly on the backbone polymer from which side chains grow. Reversible deactivation radical polymerizations such as atom transfer radical polymerization (ATRP), reversible addition-fragmentation chain transfer (RAFT) and nitroxide-mediated polymerization (NMP) are often used for this method. However, the polymers synthesized using these techniques are highly susceptible to intermolecular radical terminations during the polymerization of the side chains. This can lead to crosslinking between macromolecules and the formation of bulk gels. Because of this, BBP synthesis using the grafting-from method must be performed at dilute concentrations or terminated at low monomer conversions. While this is a major disadvantage of the grafting-from method, Matyjaszewski et al. have developed a method using catalyzed radical termination in ATRP of acrylates to avoid gelation through the suppression of chains terminated through radical combination.

1.8 Summary

SWNTs are an exceptional nanomaterial with many unique properties. However, their self-aggregation has long served as a major obstacle to their application. With increasing strategic designs of polymers and other dispersants, this obstacle has been tackled through different forms of CNT functionalization. Of these, conjugated polymers present a dual advantage: they are able to prevent bundling and allow for a unique opportunity to tune CNT properties. Design of polymer by way of architecture is an exciting avenue for SWNT functionalization. Specifically, the use of graft copolymers (which can adopt various topologies and conformations depending on their functionalities, synthetic route, and environment) to prepare a library of "hairy" supramolecular structures with a SWNT at the core is a relatively unexplored area of interest. Building on previous work in this field, this thesis aims to visualize dispersed SWNTs with graft copolymers by AFM. Architectural properties imparted on CNTs using this method may serve as a foundation for future SWNT alignment applications.

Walled Carbon Nanotubes

Chapter 2: Advanced Polymer Architecture for Preparation of Hairy Single-

The principal objective of this work is to produce a series of supramolecular structures wherein increasing molecular weights of methoxy poly(ethylene) glycol (mPEG) chains emanate from a central SWNT core. This will be accomplished by synthesizing a series of graft copolymers that can disperse SWNTs in both THF and water. Further, by taking advantage of the unique architectural arrangement of graft copolymers, this work will generate Atomic Force Microscopy (AFM) images of both the polymer and the resulting SWNT dispersion. To accomplish this experimentally, four graft copolymers will be synthesized. Poly(fluorene) will make up the backbone. To this backbone, by way of strain promoted azide alkyne cycloaddition (SPAAC), dibenzocyclooctyne (DBCO) end-group containing mPEG chains of molecular weights 5, 10, 20 and 40 kDa will be covalently bonded. Beyond AFM, these polymers and dispersions will be characterized using Fourier Transform Infrared Spectroscopy (FTIR), Thermogravimetric Analysis (TGA), and UV-Vis-NIR

2.1 Synthesis of Backbone

and Raman Spectroscopy.

The synthesis of azide-decorated polyfluorene (PF-N₃) was performed using previously established procedures (**Scheme 1**).81

NBS, HBr AcOH

r.t.

73%

Fluorene

1-bromododecane KOH, Toluene, nBu₄NBr

$$60^{\circ}$$
C

 45%

BrC₆H₁₂ C₆H₁₂Br

2

1-bromododecane KOH, Toluene, nBu₄NBr

 78%

Br AcOH

 60° C

 78%
 80° C

 78%
 80° C

 70
 70
 70
 70
 70
 70
 70
 70
 70
 70
 70
 70
 70
 70
 70
 70
 70
 70
 70
 70
 70
 70
 70
 70
 70
 70
 70
 70
 70
 70
 70
 70
 70
 70
 70
 70
 70
 70
 70
 70
 70
 70
 70
 70
 70
 70
 70
 70
 70
 70
 70
 70
 70
 70
 70
 70
 70
 70
 70
 70
 70
 70
 70
 70
 70
 70
 70
 70
 70
 70
 70
 70
 70
 70
 70
 70
 70
 70
 70
 70
 70
 70
 70
 70
 70
 70
 70
 70
 70
 70
 70
 70
 70
 70
 70
 70
 70
 70
 70
 70
 70
 70
 70
 70
 70
 70
 70
 70
 70
 70
 70
 70
 70
 70
 70
 70
 70
 70
 70
 70
 70
 70
 70
 70
 70
 70
 70
 70
 70
 70
 70
 70
 70
 70
 70
 70
 70
 70
 70
 70
 70
 70
 70
 70
 70
 70
 70
 70
 70
 70
 70
 70
 70
 70
 70
 70
 70
 70
 70
 70
 70
 70
 70
 70
 70
 70
 70
 70
 70
 70
 70
 70
 70
 70
 70
 70
 70
 70
 70
 70
 70
 70
 70
 70
 70
 70
 70
 70
 70
 70
 70
 70
 70
 70
 70
 70
 70
 70
 70
 70
 70
 70
 70
 70
 70
 70
 70
 70
 70
 70
 70
 70
 70
 70
 70
 70
 70
 70
 70
 70
 70
 70
 70
 70
 70
 70
 70
 70
 70
 70
 70
 70
 70
 70
 70
 70
 70
 70
 70
 70
 70
 70
 70
 70
 70
 70
 70
 70
 70
 70
 70
 70
 70
 70
 70
 70
 70
 70
 70
 70
 70
 70
 70
 70
 70
 70
 70
 70
 70
 70
 70
 70
 70
 70
 70
 70
 70
 70
 70
 70
 70
 70
 70
 70
 70
 70
 70
 70
 70
 70
 70
 70
 70
 70
 70
 70
 70
 70
 70
 70
 70
 70
 70

$$2 + 4 \xrightarrow{ \begin{array}{c} [(o \text{-tolyl})_3 P]_2 P d \\ \text{Toluene} \\ 3M \ K_3 P O_4 \\ 92\% \end{array} } \xrightarrow{ \begin{array}{c} Br C_6 H_{12} \\ C_6 H_{12} Br \\ C_{12} H_{25} \\ C_{12} H_{25} \end{array} } \xrightarrow{ \begin{array}{c} NaN_3, \ ^1Bu_4 NBr \\ 70^{\circ}C \\ 72\% \end{array} } \xrightarrow{ \begin{array}{c} N_3 C_6 H_{12} \\ C_6 H_{12} N_3 \\ C_{12} H_{25} \\ C_{12} H_{25} \\ \end{array} } \xrightarrow{ \begin{array}{c} C_{12} H_{25} \\ C_{12} H_{25} \\ \end{array} }$$

Scheme 1. Preparation of backbone polymer, poly(fluorene) with pendent azide groups (PF- N_3).

Briefly, commercially purchased fluorene brominated was using Nbromosuccinimide under acidic conditions to yield dibrominated fluorene (1). This was followed by two alkylations under phase-transfer conditions using 1,6-dibromohexane to yield white crystals of co-monomer 2 and using 1-bromododecane to yield monomer precursor 3. Miyaura borylation was performed using 3 to yield white crystals of comonomer 4. Suzuki-Miyaura polycondensation of co-monomers 2 and 4 afforded PF-Br (5). The final M_n of the polymer was determined by gel permeation chromatography to be 38.7 kDa, resulting in a degree of polymerization of ~42, with a dispersity of 2.1 (Figure S9). Compound 6 (PF-N₃) was prepared by substituting the alkyl bromides in PF-Br (5) with azide groups using tetrabutylammonium azide generated *in situ*. Confirmation of the azide substitution was realized through ¹H NMR where protons closest to the azide integrating for 4 experience a slight upfield shift (**Figure 11**). Fourier Transform Infrared Spectroscopy (FTIR) shows a sharp signal at ~2090 cm⁻¹ post-azide substitution on PF-Br, which is indicative of the presence of azide groups (**Figure 11**).

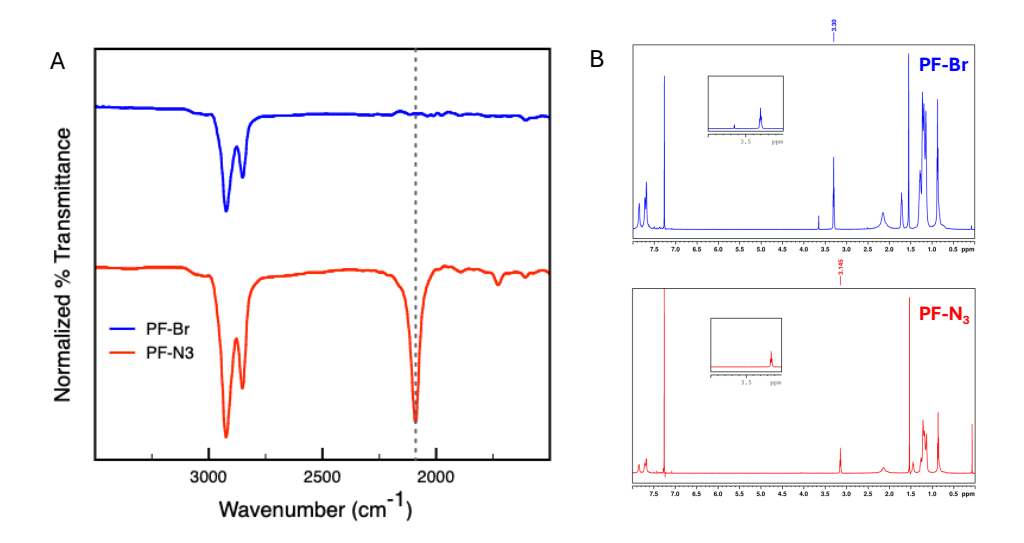


Figure 11. FTIR spectra (A) of PF-Br and PF-N₃ indicating the appearance of a sharp stretch at ~2090 cm⁻¹ corresponding to the azide group (dotted line). FTIR spectra normalized to fit in the 0-1% transmittance range. ¹H NMR spectra (B) of PF-Br and PF-N₃ showing the upfield shift of protons with the substitution to the azide groups. Both spectra calibrated to the residual solvent peak at 7.26 ppm. Insets show a closer look at the peaks of interest.

2.2 Synthesis of Side Chains

Four molecular weights of methoxy-PEG-amine were used for the synthesis of four graft copolymers; these include 5,000, 10,000, 20,000 and 40,000 g/mol.

$$O(-)$$
 $NH_2 + O(-)$ $O(-)$ $O(-)$

Scheme 2. Preparation of graft chains using mPEG-amines of molecular weights 5 (**8A**), 10 (**8B**), 20 (**8C**), and 40 kDa (**8D**).

Compound **8A-D** was prepared by an amidation reaction, modified from literature procedure. ⁸² The mPEG-amine (0.2 g, 0.04 mmol) was reacted with 2 equivalents of DBCO-NHS (0.032g, 0.08 mmol) in minimal DCM (0.74 mL) under ambient conditions. This was followed by the addition of triethylamine (17 μL). After 3 hours of stirring, the solution was precipitated using cold 1:1 hexanes:diethyl ether (40 mL) and collected by vacuum filtration to afford a white powder. Once dry, the powder was dissolved in 3.5-4 mL of DI water and filtered through a PES membrane. The filtered solution was concentrated by nitrogen blowdown evaporation then precipitated once more using cold 1:1 hexanes:diethyl ether (40 mL) and collected by vacuum filtration to afford white crystals (8A:35-66%, 8B:55-63%, 8C: 49-61%, 8D: 64%) (Scheme 2).

31

2.3 Strain Promoted Azide-Alkyne Cycloaddition

The graft copolymers (9A-D) were synthesized by strain-promoted azide alkyne cycloaddition (Scheme 3).

Scheme 3. Preparation of graft copolymers (PF-*g*-mPEG) via strain-promoted azide alkyne cycloaddition.

A concentrated solution of PF-N₃ **(6)** (4.7 mg, 0.005 mmol) in DCM (1 mL) was prepared. To this solution, mPEG-DBCO (**8A-D**) (54 mg, 0.01 mmol) was introduced and allowed to stir for 5 minutes under ambient conditions. At the 5-minute mark, the solution was triturated into cold 1:1 hexanes:diethyl ether (20 mL) and collected by vacuum filtration. The collected solid was allowed to dry *in vacuo* at 45 °C overnight, yielding the product as a powder (**9A**: 38-69%, **9B**: 70%, **9C**: 69-74%, **9D**: 74-79%) (**Scheme 3**).

32

2.4 Characterization of Graft Copolymers

The successful synthesis of the desired graft copolymers was confirmed first through an initial FTIR spectrum, then ¹H NMR, TGA curves and finally with AFM images.

2.4.1 FTIR spectra

An initial FTIR spectrum of the PF- N_3 backbone shows a sharp stretch at ~2090 cm⁻¹ corresponding to azide groups. After 5 minutes of stirring at ambient conditions in the presence of the mPEG-DBCO side chain (of molecular weights 5, 10, 20 or 40 kDa), the sharp stretch completely disappears. This indicates a complete consumption of azide groups on the poly(fluorene) backbone (**Figure 12**).

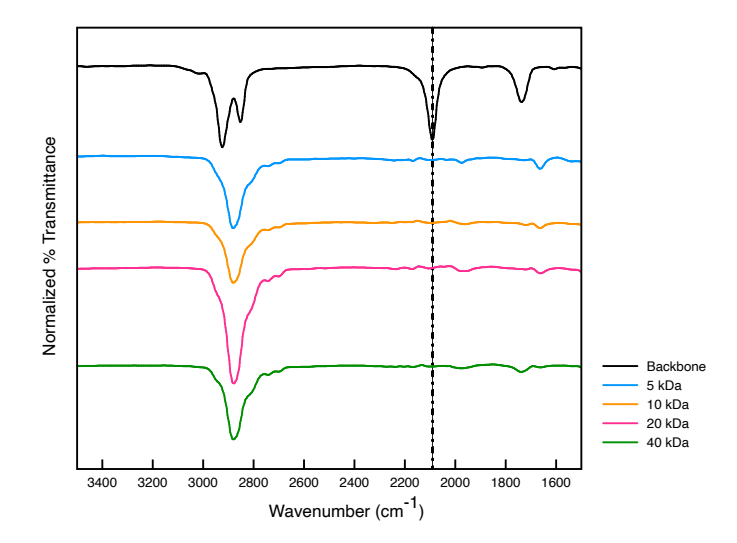


Figure 12. FTIR spectra of all graft copolymers after SPAAC, indicating the disappearance of the azide stretch at ~2090 cm⁻¹ (marked by the dotted line) after 5 minutes. Spectra normalized to fit in the 0-1% transmittance range.

2.4.2 ¹H NMR spectra

Proton NMR of the synthesized graft copolymers may not be conclusive owing to the large size of the macromolecules. A lower tumbling rate resulting from the large size of the molecule means the spectrum shows broader signals and can generate inaccurate integrations.

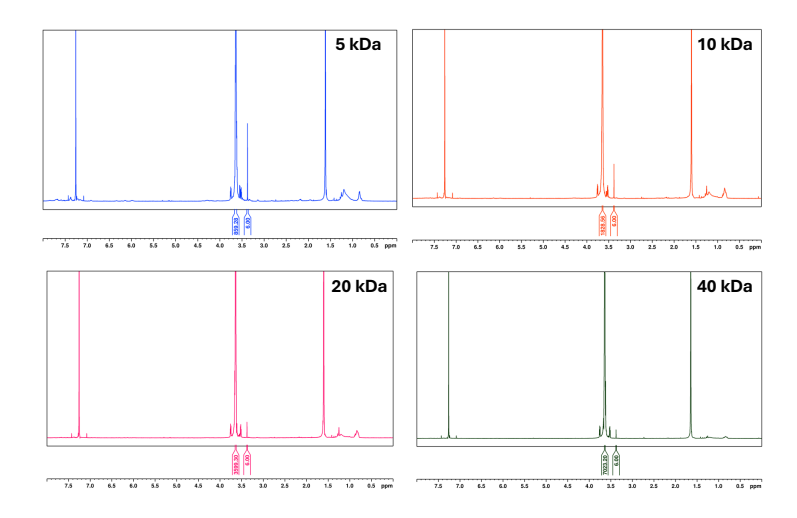


Figure 13. ¹H NMR spectra of graft copolymers in CDCl₃ (calibrated to 7.26 ppm) indicating an increase in protons attributed to the mPEG side chains.

Nevertheless, the steady increase in the protons attributed to the mPEG chains in the NMR can be used along with additional characterization to conclude the desired macromolecule has been synthesized. As seen in **Figure 13**, the protons increase from 859 for the polymer with 5 kDa side chains to 1829 for the 10 kDa side chains to 3599 for the 20 kDa side chains and finally, 7023 for the 40 kDA side chains. All NMRs have been shift-referenced to the residual CHCl₃ peak at 7.26 ppm and integrations were calibrated to the peak at ~3.4 ppm accounting for the methyl protons (6H) at the ends of the two mPEG side chains.

2.4.3 Thermogravimetric Analysis (TGA) Curves

Graft copolymers were analyzed using Thermogravimetric Analysis under an Argon atmosphere. The thermal decomposition profiles of all four graft copolymers shows a single decomposition event at ~360 °C. This event corresponds to the loss of the mPEG side chains on the backbone poly(fluorene).

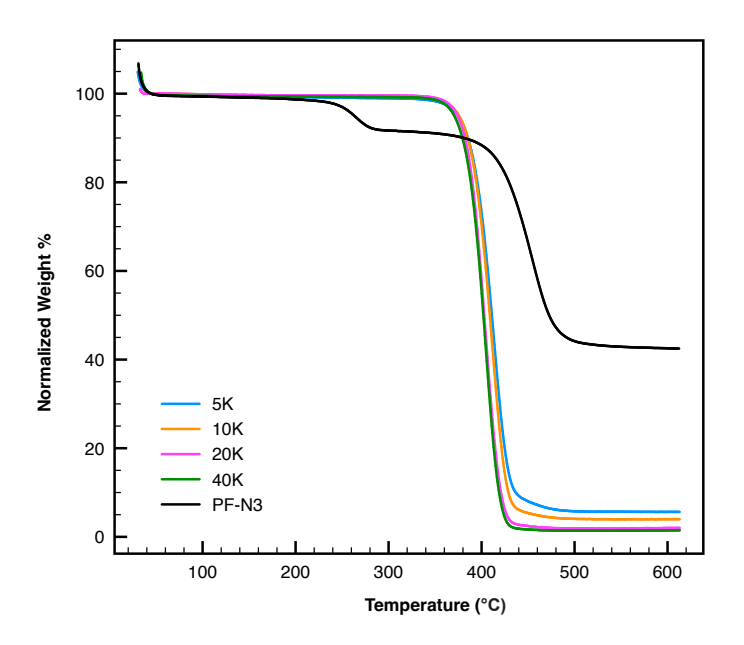


Figure 14. Thermogravimetric analysis curves of all graft copolymers along with backbone polymer.

The TGA curves of the four polymers (**Figure 14**) illustrate an increase in the mass loss of the side chains with increasing PEG length. This was expected because as the side chain molecular weight increases, there is a decrease in the amount of backbone polymer present. According to theoretical calculations (detailed in A6.1 Theoretical Calculations for TGA Curves), the graft copolymer with 5 kDa side chains should have a mass loss of 91.5%, 10 kDa should have 95.6%, 20 kDa should have 97.7% and 40 kDa should have 98.8% (**Table 1**).

Experimental TGA curve results reflect the theoretical values in that there is an increase in mass loss, as expected. The small difference between 20 kDa and 40 kDa side chain polymers may be attributed to the small difference in theoretical values, which only amounts to 1%. Such a small discrepancy becomes difficult to distinguish using TGA.

Table 1. Tabulated mass loss percentages of each graft copolymer as derived from TGA curves (**Figure 14**) along with the calculated theoretical mass loss percentages.

Graft copolymer side chain M _n	Experimental Mass Loss Percentage	Theoretical Mass Loss Percentage
5 kDa	88.4%	91.5%
10 kDa	92.0%	95.6%
20 kDa	95.6%	97.7%
40 kDa	95.9%	98.8%

2.4.4 Atomic Force Microscopy Images

To prepare samples for AFM imaging, all graft copolymers were solubilized in THF (2 mg/2mL). From this solution, either 20 or 40 μ L was spin-cast onto a silicon substrate. Images of the graft copolymers indicate distinct conformational differences as the side chain molecular weight increases. There is a visible change in the supramolecular assembly of the polymers when the polymer with 5 kDa side chains is compared to that of the 40 kDa side chains (**Figure 15**). The dark spaces represent the side chains while the bright spaces are the backbone. As molecular weight increases, the individual polymer macromolecules are repelling from one another creating different topographical behaviours.

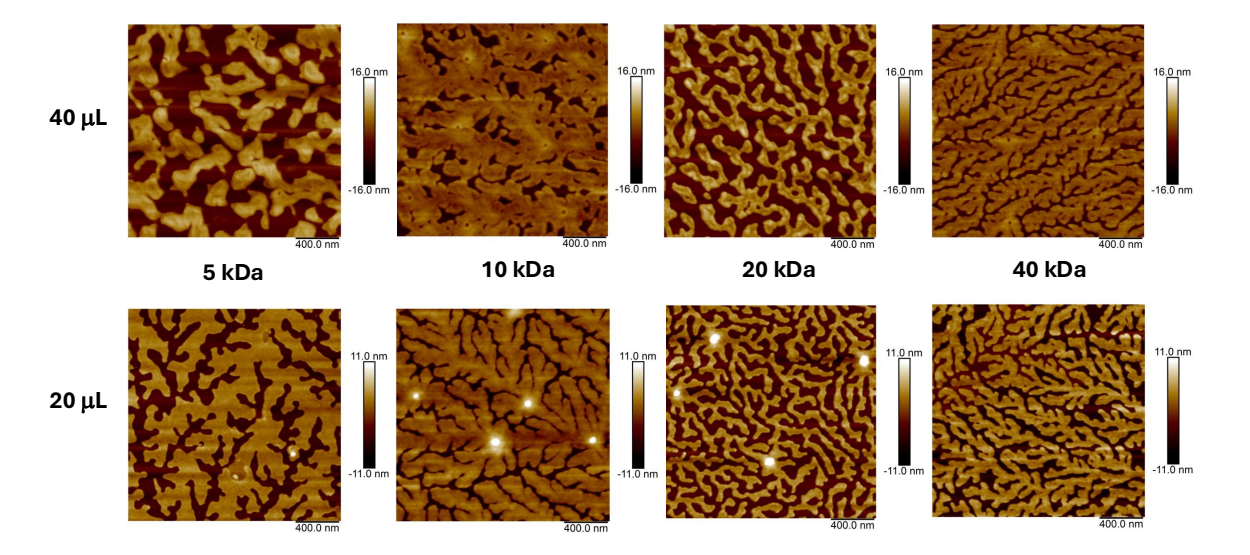


Figure 15. AFM images of all four graft copolymers showing a conformational change as the side chain increases in molecular weight. Samples of 20 or 40 μ L (as labelled) were spin-cast onto silicon from a solution of 2mg/2mL in THF.

Additionally, the categorical proof for the successful click coupling of these polymers is the absence of any globular conformations between the four graft copolymers. Whereas a PF-N₃ backbone polymer (a linear polymer) in THF would appear in a globular conformation (Figure S10) (even in a good solvent), these graft copolymers were not expected to form that conformation. As previously detailed, it is believed that the addition of grafted chains to the backbone polymer restricts the conformations that a graft polymer can take. Of the four conformations outlined in Figure 8, it is believed that these polymers are exhibiting a cylindrical conformation by compacting. This conformation is described as a desorption of the side chains wherein they repel each other. It's clear that an increase in molecular weight creates space between the macromolecules which could be attributed to the repulsion between the side chains. With the increase in molecular weight, a stronger repulsion occurs.

2.5 Preparation of PF-PEG-SWNT Dispersions

Dispersions of SWNTs using conjugated polymers have traditionally been prepared using a 1:1.5 mass ratio of polymer:SWNT. 55 However, owing to the gradual increase in the molecular weight of side chains of each graft copolymer, the backbone polymer becomes more and more dilute. This translates to a decrease in the amount of conjugated polymer that is able to interact with the surface of the SWNT. Since the π - π stacking interaction between the conjugated backbone and the SWNT surface drives the formation of dispersed SWNTs, dilution of the backbone poses a major issue. First, too little conjugated polymer leads to the possibility and wrong conclusion that a specific graft copolymer is unable to disperse SWNTs. Second, it does not allow for an equal comparison between the dispersed SWNTs using each graft copolymer. The difference in the amount of backbone polymer in each sample introduces an additional variable on top of the difference in molecular weight of the side chains.

2.5.1 Determining Equal Concentration of Backbone Polymer

For these reasons, dispersions of SWNTs using the synthesized graft copolymers were prepared by first determining an equal concentration of backbone (PF-N₃) polymer in each sample. Since the PF-N₃ has an absorbance peak at ~393 nm, UV-Vis spectroscopy was used to achieve an equal absorbance of PF-N₃ in each graft copolymer sample. Absorbance was correlated with concentration and subsequently mass using the Beer-Lambert equation (see Appendix and A6.2 Extinction Coefficient and Mass Calculation of PF-N₃ in Graft Copolymers for detailed calculations). An initial calculation was performed to determine theoretical masses of polymers that would result in equal concentration of PF-

 N_3 backbone for all four graft copolymers. These were determined to be 2.1 mg (5 kDa), 3.9 mg (10 kDa), 7.5 mg (20 kDa), 14.7 mg (40 kDa). These masses were the starting points for determining equal concentration of the backbone using the UV-Vis spectrophotometer.

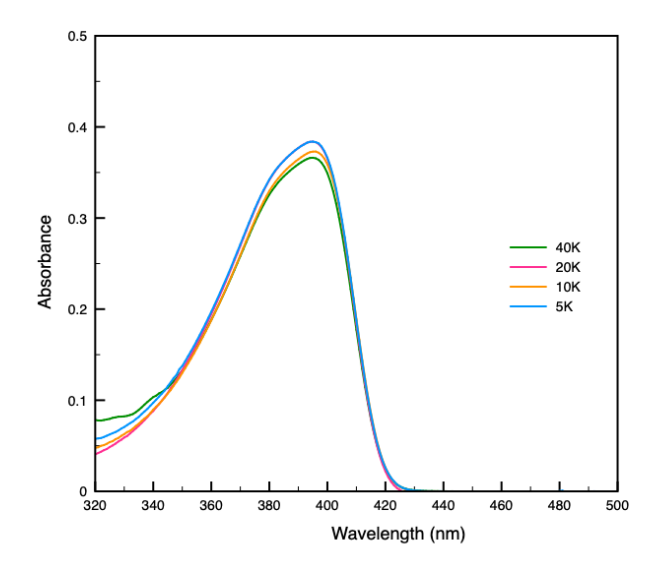


Figure 16. UV-Vis absorption spectra of graft copolymers indicating the absorbance of PF- N_3 in each sample.

The absorption spectra show peaks of PF-N₃ (~393 nm) with relatively equal absorbances in each graft copolymer (**Figure 16**). The resultant masses of each graft copolymer corresponding to the absorption spectra are outlined in **Table 2**.

Table 2. Tabulated masses of graft copolymers and SWNTs along with solvent volumes used for preparation of dispersions.

Graft Copolymer Side Chain Mn	THF Volume (mL)	Graft Copolymer (mg)	10% w/v HiPCo SWNT (mg)
5 kDa	10	3	5
10 kDa	10	4.5	5
20 kDa	10	11.2	5
40 kDa	10	24.6	5

With the determination of equal concentration of PF-N₃ in each sample, the mass of SWNTs as well as the volume of THF was kept consistent throughout all samples (as indicated in **Table 2**). The mixtures with SWNTs, graft copolymer and THF were probe sonicated for 30 mins followed by centrifugation at 8340 g for 30 mins (to remove undispersed SWNTs). The supernatant was collected after centrifugation and passed through a cotton plug. For removal of excess polymer, the dispersions were vacuum filtered through a 0.2 µm pore diameter Teflon membrane and repeatedly washed with THF until the filtrate was no longer fluorescing under a hand-held UV lamp at 365 nm. The resultant film was re-dispersed by probe sonication for 30 mins, followed by re-centrifugation at 8340 g for 30 mins and the supernatant was again collected and passed through a cotton plug to achieve the final dispersion in THF (Figure 17(B)). For dispersions in water, 4 mL of the THF dispersion was transferred to a new vial and 4 mL of DI water was mixed with this dispersion. THF was evaporated from this mixture using a rotary evaporator at 65°C. After the THF had

evaporated, the mixture left in the vial was passed through a cotton plug and the final dispersion in water was achieved (**Figure 17** (A)).

2.6 Characterization of SWNT Dispersions

Qualitatively, based on the appearance of the dispersions, it can be determined that all four graft copolymers were able to disperse HiPCo SWNTs in Water and THF. Whereas all four polymers presented dark coloured dispersions in THF, in water the lowest molecular weight polymer (with side chains of 5 kDa) was unable to form a dark/black coloured dispersion. This can be attributed to the fact that water is a poor solvent for SWNT dispersion and the smaller side chains of the polymer are unable to provide enough steric barrier between individual nanotubes in order to separate and stabilize the nanotube dispersions as the solvent is exchanged.





Figure 17. Dispersions of SWNTs using graft copolymers with increasing molecular weights of side chains (left to right: 5, 10, 20, 40 kDa) in Water (A) and THF (B).

2.6.1 UV-Vis-NIR Spectra of SWNT Dispersions in Water and THF

As previously discussed, UV-Vis-NIR spectroscopy allows for the examination of concentration, purity and chirality of SWNT dispersions. Visually, from photographs of the dispersions (**Figure 17**), it is evident that the graft copolymers were successful at dispersing SWNTs. The UV-Vis spectra (**Figure 18**) also show that there are SWNTs in the dispersions. Further, these spectra show that none of the graft copolymers, regardless of the solvent used, were selective toward any one chirality and consequently metallic or semiconducting nature of the SWNTs. The spectra also show that the graft copolymers with 5 kDa side chains dispersed the lowest amount of SWNTs in both solvents. This follows the expected behaviour of lower molecular weight polymers which form more dilute dispersions compared to their higher molecular weight counterparts.

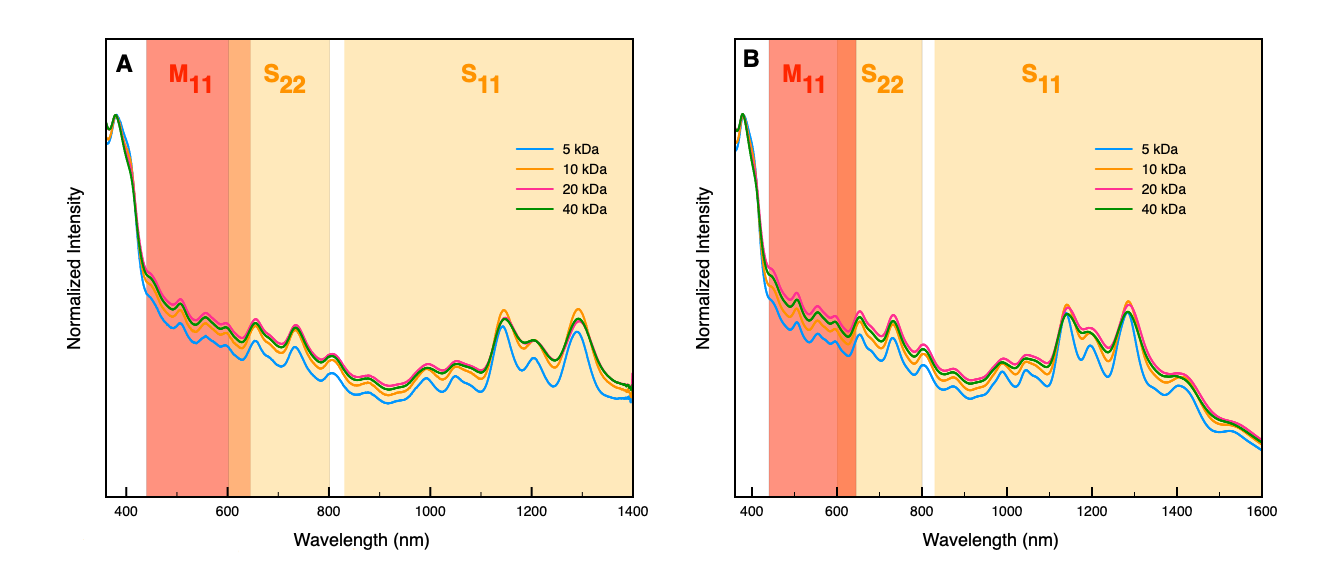


Figure 18. UV-Vis-NIR spectra of dispersions in water (A) and THF (B) using graft copolymers. All spectra normalized to 380 nm.

2.6.2 Resonance Raman Spectra of SWNT Dispersions in Water and THF

All Raman samples were prepared by drop casting one drop of dispersion onto a silicon substrate. Analysis was performed by applying lasers with excitation wavelengths of 532, 633 and 785 nm. The full Raman spectra of all dispersions in THF and Water are seen in **Figure 19**. The G-band exhibits a Lorentzian line shape in all samples, indicating the presence of sc-SWNTs.

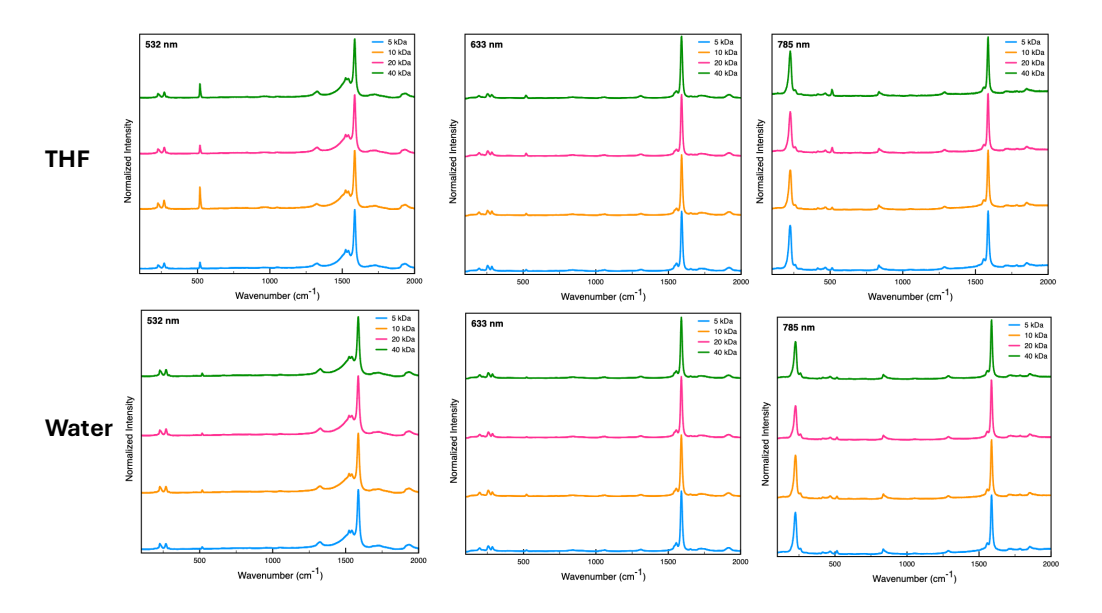


Figure 19. Full Raman spectra of dispersions using all four graft copolymers in THF and water. Spectra with λ_{ex} = 532 nm was normalized to ~1586 cm⁻¹, with λ_{ex} = 633 was normalized to ~1591 cm⁻¹ and with λ_{ex} = 735 was normalized to 1587 cm⁻¹. The peak at 520 cm⁻¹ corresponds to the silicon substrate.⁵⁵

The RBM region of all samples is seen in **Figure 20**. The spectra derived from using the 532 nm wavelength only has metallic SWNTs in resonance. The spectra reflect this as only m-SWNTs are seen.⁵⁵ Excitation using the 633 nm wavelength has both both m- and sc-SWNTs in resonance. Based on the spectra, it is evident that the graft copolymers are not selective

toward any diameter or electronic nature of SWNTs as both sc- and m-SWNTs are present on all spectra regardless of solvent used. Finally, excitation at 785 nm can show the presence of bundling with a peak at 265 nm, which accounts for the (10, 2) SWNT species. ⁵⁵ Based on the spectra (**Figure 20**), the peak intensity at 265 cm⁻¹ in comparison to the primary peak is low. This indicates low bundling, if any, and the successful dispersion of SWNTs.

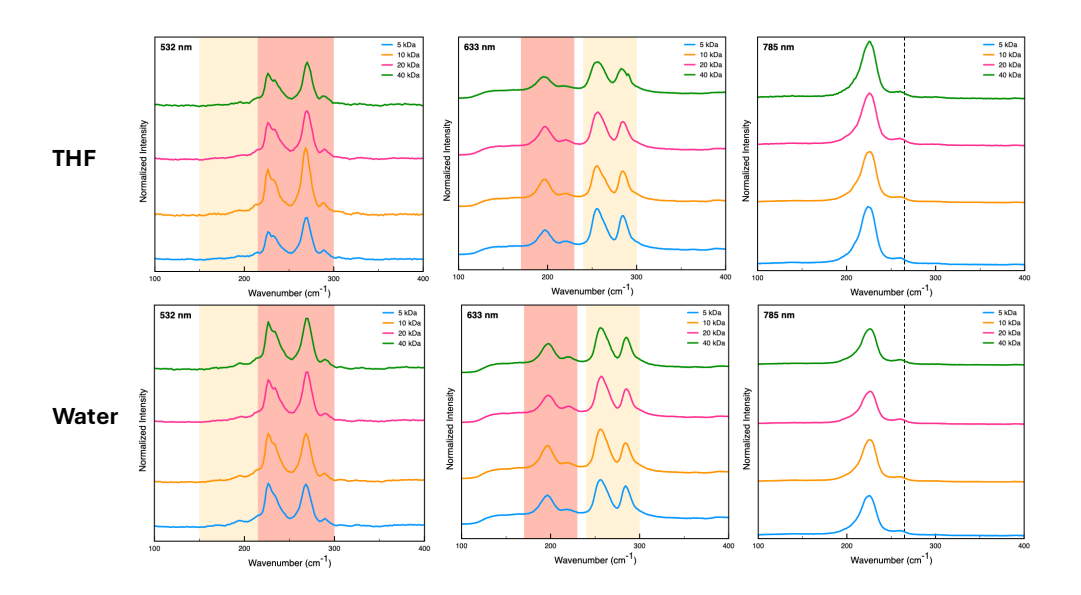


Figure 20. RBM region of Raman spectra from **Figure 19** of dispersions using all four graft copolymers in THF and water. Spectra with λ_{ex} = 532 nm was normalized to ~1586 cm⁻¹, with λ_{ex} = 633 was normalized to ~1591 cm⁻¹ and with λ_{ex} = 735 was normalized to 1587 cm⁻¹. Red boxes highlight m-SWNTs, and yellow boxes highlight sc-SWNTs. Dotted line represents the signal for SWNT bundling (265 cm⁻¹).⁵⁵

2.6.3 Atomic Force Microscopy Images of SWNT Dispersions

To prepare dispersion samples for AFM imaging, 20 µL of the dispersion in THF was spin-cast onto a silicon substrate. The images (**Figure 21**) show distinct differences between the four samples. While there is no real alignment or arrangement of SWNTs, there are some

topographical differences. As the molecular weights of the side chains increase, polymer-SWNT complexes look less and less like straight rods. This difference is most obvious between the 10 kDa and 40 kDa samples.

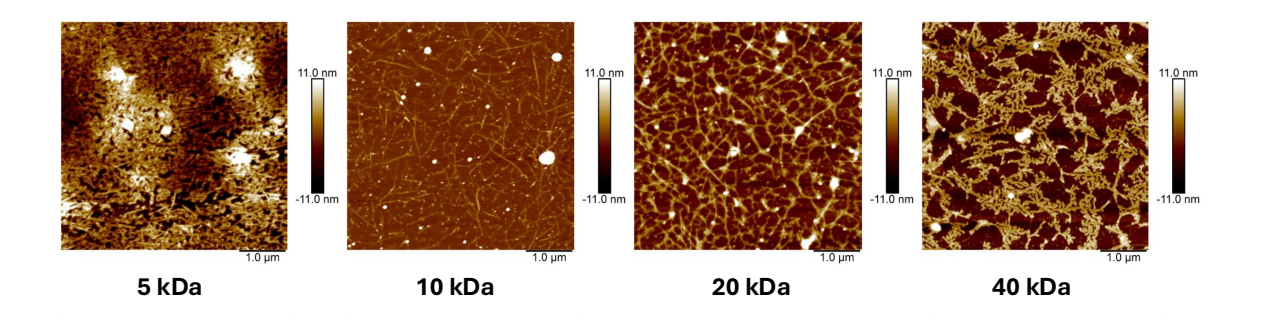


Figure 21. AFM images of dispersions in THF using graft copolymers.

The 5 kDa side chain graft copolymer was difficult to visualize on AFM. Despite several trials, the silicon surface appeared to have a film-like layer on top after spin-coating. Repeated imaging via AFM showed no signs of SWNTs present on the surface (**Figure S12**). From other characterization techniques described previously and qualitatively it is evident that SWNTs were dispersed with the 5 kDa graft copolymer. This means that the sample does contain SWNTs and these should be visualized by AFM (as has been shown for all other molecular weight polymers). A potential explanation for this behaviour is that after dispersion of SWNTs, the grafted chains on the polymer are desorbed from the surface and form an attraction to each other resulting in a globular conformation. This could prevent

M.Sc. Thesis – Unnati Desai McMaster University – Chemistry and Chemical Biology adsorption on the silicon surface and create aggregation of any macromolecules which are adsorbed. This may also explain why no SWNTs are seen.

Chapter 3: Conclusions and Recommendation for Future Work

3.1 Conclusion

SWNTs are an important allotrope of carbon that have many exceptional properties. One major caveat is their self-aggregation resulting in poor dispersibility and consequently poor applicability of SWNTs. Conjugated polymers have stood out as an apt solution for this issue because of their ability to form strong π - π stacking interactions with the surface of the SWNT and impart additional tunable properties.

By preparing conjugated polymers into advanced architectures, this thesis shifted focus from conjugated polymers' chemical tunability to architectural design. A library of graft copolymers was synthesized using increasing molecular weights of mPEG-amine grafted chains. It was shown that the synthesis of these polymers was efficient through SPAAC. These polymers were used to prepare supramolecular structures in the form of "hairy" SWNTs. The graft copolymer library was able to successfully disperse SWNTs and impart new properties (aqueous dispersibility). Beyond dispersibility, it was shown that the unique architectural difference, visualized by AFM, of the graft copolymers could serve as a basis for imparting topographical changes to SWNT dispersions.

3.2 Recommendation for Future Work

To build on this work, increasing the grafting density of the graft copolymers synthesized here would serve as an exciting next step. As has been discussed previously, grafting density of graft polymers is a key parameter in determining conformational changes. To induce even more architectural differences within the polymers synthesized, it would be beneficial to use a polymer that can carry even more grafted chains than has been presented in this thesis. One way would be to synthesize a homopolymer instead of the co-polymer used here. Beyond this, the ability of these polymers to disperse SWNTs in water opens the possibility for biological applications. Using click chemistry to conjugate different biological moieties to these graft copolymers could prove beneficial for applications in drug delivery and biosensing. The work presented in this thesis can serve as a foundational beginning to a whole array of different pathways from strategic architectural design of polymers to biological modifications.

References

- 1. Iijima, S., Helical microtubules of graphitic carbon. *Letters to Nature* **354** (1991).
- 2. Park, S., Vosguerichian, M. & Bao, Z. A review of fabrication and applications of carbon nanotube film-based flexible electronics. *Nanoscale* **5**, 1727 (2013).
- 3. Kolahdouz, M. et al. Carbon-Related Materials: Graphene and Carbon Nanotubes in Semiconductor Applications and Design. *Micromachines* 13, 1257 (2022).
- Thostenson, E. T., Ren, Z. & Chou, T.-W. Advances in the science and technology of carbon nanotubes and their composites: a review. Compos. Sci. Technol. 61, 1899–1912 (2001).
- 5. Chen, J., Liu, B., Gao, X. & Xu, D. A review of the interfacial characteristics of polymer nanocomposites containing carbon nanotubes. RSC Adv. 8, 28048–28085 (2018).
- 6. Hughes, K. J. et al. Review of Carbon Nanotube Research and Development: Materials and Emerging Applications. ACS Appl. Nano Mater. 7, 18695–18713 (2024).
- 7. Hirsch, A. Functionalization of Single-Walled Carbon Nanotubes. Angew. Chem. Int. Ed. 41, 1853 (2002).
- 8. De Volder, M. F. L., Tawfick, S. H., Baughman, R. H. & Hart, A. J. Carbon Nanotubes: Present and Future Commercial Applications. Science 339, 535–539 (2013).
- 9. Hersam, M.C. Progress towards monodisperse single-walled carbon nanotubes. Nature Nanotechnology 3 (2008).
- 10. Zhou, W., Bai, X., Wang, E. & Xie, S. Synthesis, Structure, and Properties of Single-Walled Carbon Nanotubes. Adv. Mater. 21, 4565–4583 (2009).
- 11. Bahr, J. L. & Tour, J. M. Covalent chemistry of single-wall carbon nanotubes. J. Mater. Chem. **12**, 1952–1958 (2002).

- 12. Fujigaya, T. & Nakashima, N. Non-covalent polymer wrapping of carbon nanotubes and the role of wrapped polymers as functional dispersants. *Sci. Technol. Adv. Mater.* **16**, 024802 (2015).
- 13. Eatemadi, A. *et al.* Carbon nanotubes: properties, synthesis, purification, and medical applications. *Nanoscale Res. Lett.* **9**, 393 (2014).
- 14. Wilder, J. W. G., Venema, L. C., Rinzler, A. G., Smalley, R. E. & Dekker, C. Electronic structure of atomically resolved carbon nanotubes. *Nature* **391**, 59–62 (1998).
- 15. Collins, P. G. & Avouris, P. They are stronger than steel, but the most important uses for these threadlike macromolecules may be in faster, more efficient and more durable electronic devices.
- 16. Popov, V. Carbon nanotubes: properties and application. *Mater. Sci. Eng. R Rep.* **43**, 61–102 (2004).
- 17. Dresselhaus, M. S., Dresselhaus, G., Saito, R. & Jorio, A. Raman spectroscopy of carbon nanotubes. *Phys. Rep.* **409**, 47–99 (2005).
- 18. Nanot, S., Hároz, E. H., Kim, J., Hauge, R. H. & Kono, J. Optoelectronic Properties of Single-Wall Carbon Nanotubes. *Adv. Mater.* **24**, 4977–4994 (2012).
- 19. Dubey, R., Dutta, D., Sarkar, A. & Chattopadhyay, P. Functionalized carbon nanotubes: synthesis, properties and applications in water purification, drug delivery, and material and biomedical sciences. *Nanoscale Adv.* **3**, 5722–5744 (2021).
- 20. Yakobson, B. I., Brabec, C. J. & Bernholc, J. Nanomechanics of Carbon Tubes: Instabilities beyond Linear Response. *Phys. Rev. Lett.* **76**, 2511–2514 (1996).
- 21. Hu, L., Hecht, D. S. & Grüner, G. Carbon Nanotube Thin Films: Fabrication, Properties, and Applications. *Chem. Rev.* **110**, 5790–5844 (2010).

- 22. Jariwala, D., Sangwan, V. K., Lauhon, L. J., Marks, T. J. & Hersam, M. C. Carbon nanomaterials for electronics, optoelectronics, photovoltaics, and sensing. *Chem Soc Rev* 42, 2824–2860 (2013).
- 23. Rafique, M. M. A. & Iqbal, J. Production of Carbon Nanotubes by Different Routes-A Review. *J. Encapsulation Adsorpt. Sci.* **01**, 29–34 (2011).
- 24. Chiang, I. W. *et al.* Purification and Characterization of Single-Wall Carbon Nanotubes (SWNTs) Obtained from the Gas-Phase Decomposition of CO (HiPco Process). *J. Phys. Chem. B* **105**, 8297–8301 (2001).
- 25. Samanta, S.K. *et al.* Conjugated Polymer-Assissted Dispersion of Single-Wall Carbon Nanotubes: The Power of Polymer Wrapping. *Acc. Chem. Res.* **47**, 2446-2456 (2014).
- 26. Lefrant, S., Baibarac, M. & Baltog, I. Raman and FTIR spectroscopy as valuable tools for the characterization of polymer and carbon nanotube based composites. *J. Mater. Chem.* 19, 5690 (2009).
- 27. O'Connell, M. J. *et al.* Band Gap Fluorescence from Individual Single-Walled Carbon Nanotubes. *Science* **297**, 593–596 (2002).
- 28. Hirsch, A. & Vostrowsky, O. Functionalization of Carbon Nanotubes. in *Functional Molecular Nanostructures* (ed. Schlüter, A. D.) vol. 245 193–237 (Springer Berlin Heidelberg, Berlin, Heidelberg, 2005).
- 29. Norizan, M. N. *et al.* Carbon nanotubes: functionalisation and their application in chemical sensors. *RSC Adv.* **10**, 43704–43732 (2020).
- 30. Rao, R. K., Gautham, S. & Sasmal, S. A Comprehensive Review on Carbon Nanotubes Based Smart Nanocomposites Sensors for Various Novel Sensing Applications. *Polym. Rev.* 1–64 (2024).

- 31. Hwang, J.-Y. *et al.* Polymer Structure and Solvent Effects on the Selective Dispersion of Single-Walled Carbon Nanotubes. *J. Am. Chem. Soc.* **130**, 3543–3553 (2008).
- 32. Zhou, Y. *et al.* Non-Covalent Functionalization of Carbon Nanotubes for Electrochemical Biosensor Development. *Sensors* **19**, 392 (2019).
- 33. Britz, D. A. & Khlobystov, A. N. Noncovalent interactions of molecules with single walled carbon nanotubes. *Chem. Soc. Rev.* **35**, 637 (2006).
- 34. Tournus, F. & Charlier, J.-C. *Ab initio* study of benzene adsorption on carbon nanotubes. *Phys. Rev. B* **71**, 165421 (2005).
- 35. Liu, J., Moo-Young, J., McInnis, M., Pasquinelli, M. A. & Zhai, L. Conjugated Polymer Assemblies on Carbon Nanotubes. *Macromolecules* **47**, 705–712 (2014).
- 36. Bilalis, P., Katsigiannopoulos, D., Avgeropoulos, A. & Sakellariou, G. Non-covalent functionalization of carbon nanotubes with polymers. *RSC Adv* 4, 2911–2934 (2014).
- 37. Fong, D. & Adronov, A. Recent developments in the selective dispersion of single-walled carbon nanotubes using conjugated polymers. *Chem Sci* **8**, 7292–7305 (2017).
- 38. Kim, J. *et al.* A Mechanochemical Approach to Nanocomposites Using Single-Wall Carbon Nanotubes and Poly(L -lysine). *Macromol. Rapid Commun.* **28**, 767–771 (2007).
- 39. Zhao, B., Hu, H., Yu, A., Perea, D. & Haddon, R. C. Synthesis and Characterization of Water Soluble Single-Walled Carbon Nanotube Graft Copolymers. *J. Am. Chem. Soc.* **127**, 8197–8203 (2005).
- 40. Fong, D., Andrews, G. M. & Adronov, A. Functionalization of polyfluorene-wrapped carbon nanotubes *via* copper-mediated azide–alkyne cycloaddition. *Polym. Chem.* **9**, 2873–2879 (2018).

- 41. Fong, D., Yeung, J., McNelles, S. A. & Adronov, A. Decoration of Polyfluorene-Wrapped Carbon Nanotubes via Strain-Promoted Azide–Alkyne Cycloaddition. *Macromolecules* **51**, 755–762 (2018).
- 42. Sheiko, S. S., Sumerlin, B. S. & Matyjaszewski, K. Cylindrical molecular brushes: Synthesis, characterization, and properties. *Prog. Polym. Sci.* **33**, 759–785 (2008).
- 43. Bati, A. S. R., Yu, L., Batmunkh, M. & Shapter, J. G. Synthesis, purification, properties and characterization of sorted single-walled carbon nanotubes. *Nanoscale* **10**, 22087–22139 (2018).
- 44. Njuguna, J., Vanli, O. A. & Liang, R. A Review of Spectral Methods for Dispersion Characterization of Carbon Nanotubes in Aqueous Suspensions. *J. Spectrosc.* **2015**, 1–11 (2015).
- 45. Binnig, G., Quate, C. F. & Gerber, Ch. Atomic Force Microscope. *Phys. Rev. Lett.* **56**, 930–933 (1986).
- 46. Piontek, M. C. & Roos, W. H. Atomic Force Microscopy: An Introduction. in *Single Molecule Analysis* (ed. Peterman, E. J. G.) vol. 1665 243–258 (Springer New York, New York, NY, 2018).
- 47. Magonov, S. N. & Reneker, D. H. CHARACTERIZATION OF POLYMER SURFACES WITH ATOMIC FORCE MICROSCOPY. *Annu. Rev. Mater. Sci.* **27**, 175–222 (1997).
- 48. Wang, W. *et al.* The heterogeneity and electro-mechanical characteristics of coal at the micro-and nanoscale. *J. Geophys. Eng.* **16**, 717–728 (2019).
- Campbell, J. F., Tessmer, I., Thorp, H. H. & Erie, D. A. Atomic Force Microscopy Studies of DNA-Wrapped Carbon Nanotube Structure and Binding to Quantum Dots. *J. Am. Chem. Soc.* 130, 10648–10655 (2008).

- 50. Sheiko, S. S. et al. Measuring Molecular Weight by Atomic Force Microscopy. J. Am. Chem. Soc. 125, 6725–6728 (2003).
- 51. Henn, D. M., Holmes, J. A., Kent, E. W. & Zhao, B. Worm-to-Sphere Shape Transition of Thermoresponsive Linear Molecular Bottlebrushes in Moderately Concentrated Aqueous Solution. *J. Phys. Chem. B* **122**, 7015–7025 (2018).
- 52. Lord, S. J., Sheiko, S. S., LaRue, I., Lee, H.-I. & Matyjaszewski, K. Tadpole Conformation of Gradient Polymer Brushes. *Macromolecules* **37**, 4235–4240 (2004).
- 53. Potemkin, I. I. *et al.* Spontaneous Curvature of Comblike Polymers at a Flat Interface. *Macromolecules* 37, 3918–3923 (2004).
- 54. Kent, E. W., Lewoczko, E. M. & Zhao, B. Effect of Buffer Anions on Pearl-Necklace Morphology of Tertiary Amine-Containing Binary Heterografted Linear Molecular Bottlebrushes in Acidic Aqueous Buffers. *Langmuir* **36**, 13320–13330 (2020).
- 55. Kukendran, S., Salimi, S. & Adronov, A. Interaction and Click Functionalization of a Poly(Thiopenyl-Tetrazine-Co-Fluorene) Conjugated Polymer with Single-Walled Carbon Nanotubes. *Helv. Chim. Acta* **108** (2025).
- 56. Rice, N. A., Subrahmanyam, A. V., Coleman, B. R. & Adronov, A. Effect of Induction on the Dispersion of Semiconducting and Metallic Single-Walled Carbon Nanotubes Using Conjugated Polymers. *Macromolecules* **48**, 5155–5161 (2015).
- 57. Rice, N. A. & Adronov, A. Supramolecular Interactions of High Molecular Weight Poly(2,7-carbazole)s with Single-Walled Carbon Nanotubes. *Macromolecules* **46**, 3850–3860 (2013).
- 58. Mirka, B. *et al.* Polyfluorene-Sorted Semiconducting Single-Walled Carbon Nanotubes for Applications in Thin-Film Transistors. *Chem. Mater.* **31**, 2863–2872 (2019).

- 59. Sanchez, S. R., Bachilo, S. M., Kadria-Vili, Y., Lin, C.-W. & Weisman, R. B. (*n*, *m*)-Specific Absorption Cross Sections of Single-Walled Carbon Nanotubes Measured by Variance Spectroscopy. *Nano Lett.* **16**, 6903–6909 (2016).
- 60. Strano, M. S. *et al.* Electronic Structure Control of Single-Walled Carbon Nanotube Functionalization. *Science* **301**, 1519–1522 (2003).
- 61. Chandra, A. *et al.* Unveiling the Molecular Secrets: A Comprehensive Review of Raman Spectroscopy in Biological Research. *ACS Omega* **9**, 50049–50063 (2024).
- 62. Jones, R. R., Hooper, D. C., Zhang, L., Wolverson, D. & Valev, V. K. Raman Techniques: Fundamentals and Frontiers. *Nanoscale Res. Lett.* **14**, 231 (2019).
- 63. Dresselhaus, M. S. et al. Single Nanotube Raman Spectroscopy. Acc. Chem. Res. 35, 1070–1078 (2002).
- 64. Jorio, A. *et al.* Characterizing carbon nanotube samples with resonance Raman scattering. *New J. Phys.* **5**, 139–139 (2003).
- 65. Bodnaryk, W. J. Purification of Semiconducting and Metallic Single-Walled Carbon Nanotubes Using Conjugated Polymers. Ph.D. Thesis, McMaster University, 2020.
- 66. Michel, T. *et al.* Indexing of individual single-walled carbon nanotubes from Raman spectroscopy. *Phys. Rev. B* **80**, 245416 (2009).
- 67. Costa, S., Borowiak-Palen, E., Kruszyńska, M., Bachmatiuk, A. & Kaleńczuk, R. J. Characterization of carbon nanotubes by Raman spectroscopy.
- 68. Thomsen, C., Reich, S. & Maultzsch, J. Resonant Raman spectroscopy of nanotubes. *Philos. Trans. R. Soc. Lond. Ser. Math. Phys. Eng. Sci.* **362**, 2337–2359 (2004).
- 69. Bottom, R. Thermogravimetric Analysis. in *Principles and Applications of Thermal Analysis* (ed. Gabbott, P.) 87–118 (Wiley, 2008).

- 70. Hu, K., Mu, R., Ma, Z. & Li, B. Bottlebrush Polymers: From Synthesis to Properties and Applications. *Macromol. Rapid Commun.* 2500215 (2025).
- 71. Zhu, M., Pan, X., Zheng, T. & Li, L. Research progress on the conformational properties of comb-like polymers in dilute solutions. *Soft Matter* **20**, 463–483 (2024).
- 72. Liang, H. *et al.* Universality of the Entanglement Plateau Modulus of Comb and Bottlebrush Polymer Melts. *Macromolecules* **51**, 10028–10039 (2018).
- 73. Abbasi, M., Faust, L., Riazi, K. & Wilhelm, M. Linear and Extensional Rheology of Model Branched Polystyrenes: From Loosely Grafted Combs to Bottlebrushes. *Macromolecules* **50**, 5964–5977 (2017).
- 74. Zhao, B. Shape-Changing Bottlebrush Polymers. J. Phys. Chem. B 125, 6373–6389 (2021).
- 75. Ajvazi, E. *et al.* Inorganic Bottlebrush and Comb Polymers as a Platform for Supersoft, Solvent-Free Elastomers. *ACS Polym. Au* **4**, 56–65 (2024).
- 76. Sheiko, S. S. *et al.* Adsorption-induced scission of carbon–carbon bonds. *Nature* **440**, 191–194 (2006).
- 77. Paturej, J., Sheiko, S. S., Panyukov, S. & Rubinstein, M. Molecular structure of bottlebrush polymers in melts. *Sci. Adv.* **2**, e1601478 (2016).
- 78. Liang, H., Wang, Z., Sheiko, S. S. & Dobrynin, A. V. Comb and Bottlebrush Graft Copolymers in a Melt. *Macromolecules* **52**, 3942–3950 (2019).
- 79. Clarke, B. R. et al. Bottlebrush Networks: A Primer for Advanced Architectures. Angew. Chem. Int. Ed. 63, e202318220 (2024).
- 80. Xie, G., Martinez, M. R., Olszewski, M., Sheiko, S. S. & Matyjaszewski, K. Molecular Bottlebrushes as Novel Materials. *Biomacromolecules* **20**, 27–54 (2019).

- 81. Fong, D., Yeung, J., McNelles, S. A. & Adronov, A. Decoration of Polyfluorene-Wrapped Carbon Nanotubes via Strain-Promoted Azide–Alkyne Cycloaddition. *Macromolecules* **51**, 755–762 (2018).
- 82. McNelles, S. A., Marando, V. M. & Adronov, A. Globular Polymer Grafts Require a Critical Size for Efficient Molecular Sieving of Enzyme Substrates. *Angew. Chem. Int. Ed.* **58**, 8448–8453 (2019).

Appendix

A1 General Experimental

All reagents that were purchased from commercial suppliers were used as received. Raw HiPCo SWNTs were purchased from NanoIntegris (batch #HR37-139A, stored as a 10 wt% slurry in EtOH) and used without additional purification. Flash chromatography was done with a CombiFlash®R_f by Teledyne. Compounds were monitored using a variable wavelength detector at 254 nm. Columns were prepared in Biotage®SNAP KP-Sil cartridges with 40-63 µm silica or 25-40 µm silica purchased from Silicycle. ¹H NMR spectra were recorded on Bruker Advance 600 MHz and referenced to the residual solvent resonance (CHCl₃ at 7.26 ppm). Polymer molecular weights and dispersities were analyzed (relative to polystyrene standards) via GPC using a Tosoh EcoSEC Elite HLC 8420-GPC with a Tosoh dual flow refractive index detector and an ultraviolet detector. Samples were eluted through two Tosoh TSKgel SuperH-RC, 6.0 mm ID x 15 cm, 4 µm, columns equipped with a Tosoh 4.6 mm ID x 3.5 cm, 4 m, guard column. The mobile phase was THF with 2% acetonitrile at a flow rate of 0.6 mL/min. Sonication was performed using QSonica Q700 Sonicator with a 13 mm probe. A Beckman Coulter Allegra X-22 centrifuge was used for centrifugation at 8340 g. Fourier-Transform Infrared (FTIR) spectra were collected with Thermo Scientific Nicolet 6700 FT-IR spectrometer equipped with a Smart iTX attenuated total reflectance (ATR) sample analyzer. UV-vis-NIR spectra were collected on a Cary 5000 spectrometer in dual beam mode, using identical 10 mm quartz cuvettes. Raman spectra were collected using a Renishaw InVia Laser Raman spectrometer, with a 500 mW HeNe Renishaw laser (633 nm,

1800 L/mm grating), a 300 mW Renishaw laser (785 nm, 1200 L/mm grating) and a 50 mW Renishaw laser (532 nm, 1800 L/mm grating). Thermogravimetric analysis (TGA) was done on a Mettler Toledo TGA/DSC 3+, and all measurements were performed under an Argon atmosphere. Atomic Force Microscopy (AFM) images were acquired using a Bruker Dimension Icon AFM equipped with ScanAsyst-Air tips in ScanAsyst in Air Mode. Image processing (flattening, removal of errant scan lines, height profile measurements) was performed using NanoScope Analysis v.2.0. AFM samples were prepared by spin-coating onto silicon substrate at 4000 RPM.

A2 Statistical Analysis

All data was processed using Plot2x Version 2.7.3. All UV-Vis-NIR absorption and Resonance Raman spectra and ¹H NMRs were normalized and calibrated as detailed in respective captions. Schemes and chemical structures were produced using PerkinElmer ChemDraw 21.0.0.28.

A3 NMR Spectra

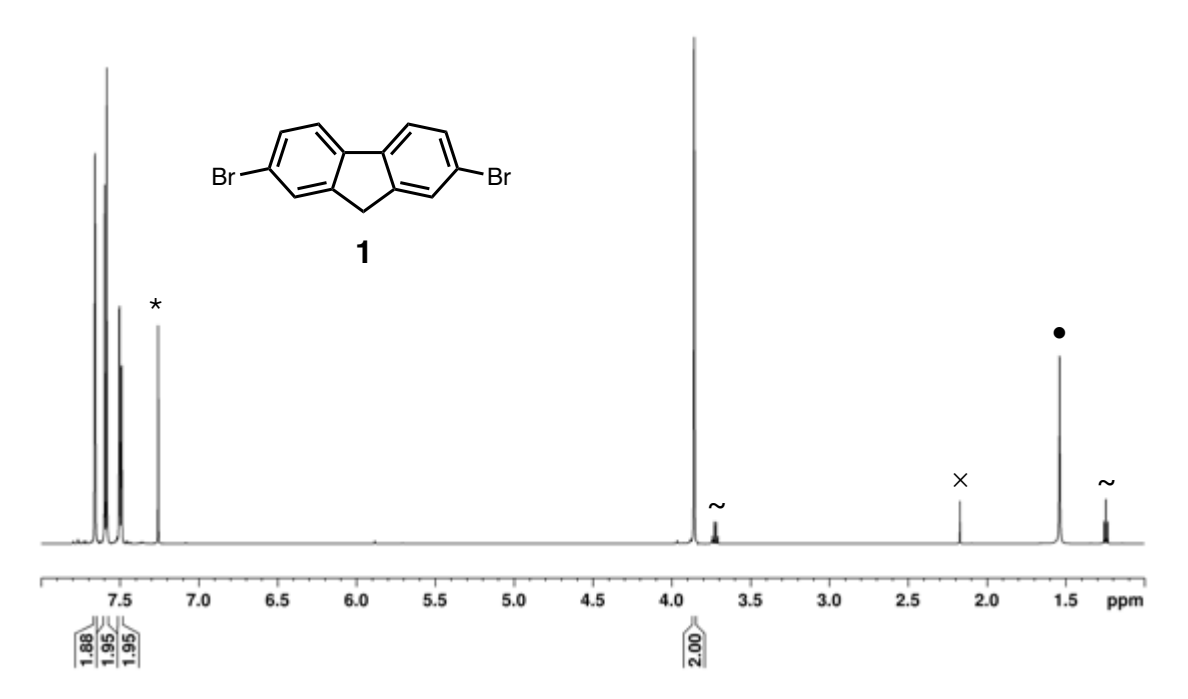


Figure S1. ¹H NMR of compound 1 in CDCl3 (*) where (~) represents ethanol, (•) represents water and (\times) represents acetone.

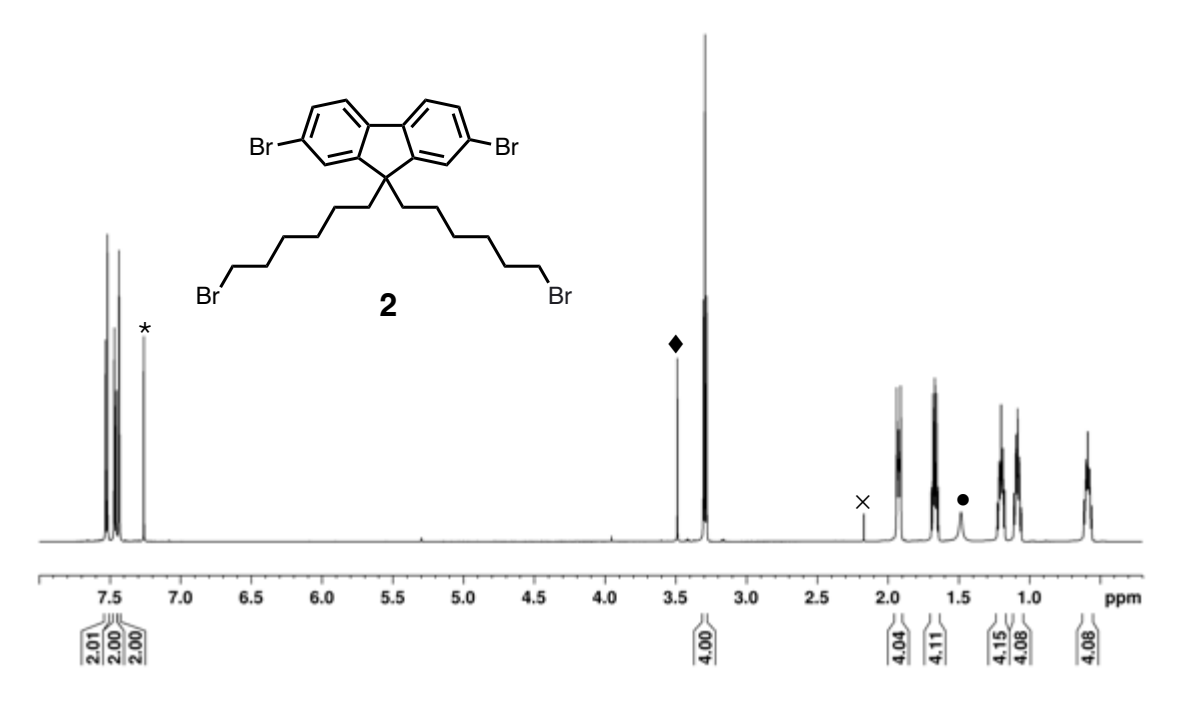


Figure S2. ¹H NMR of compound 2 in CDCl3 (*) where (×) represents acetone, (•) represents water and (♦) represents methanol.

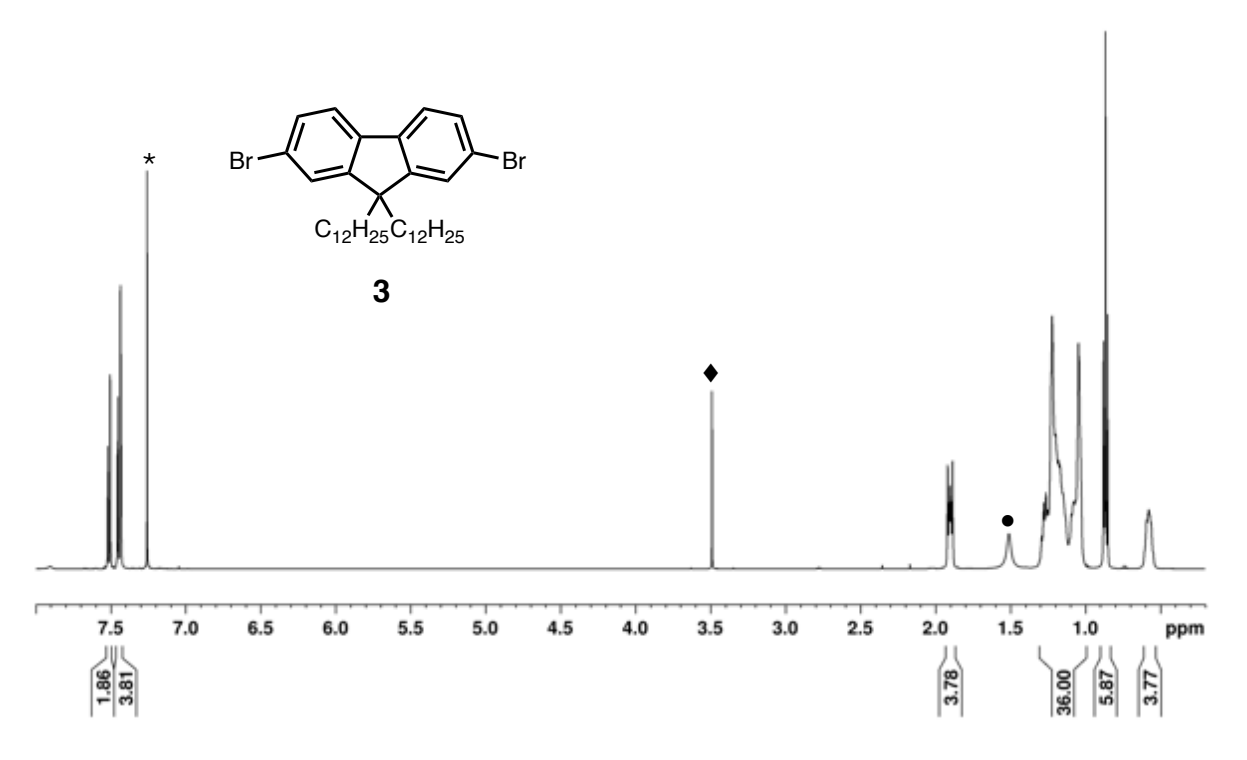


Figure S3.¹H NMR of compound 3 in CDCl₃ (*) where (•) represents water and (♦) represents methanol.

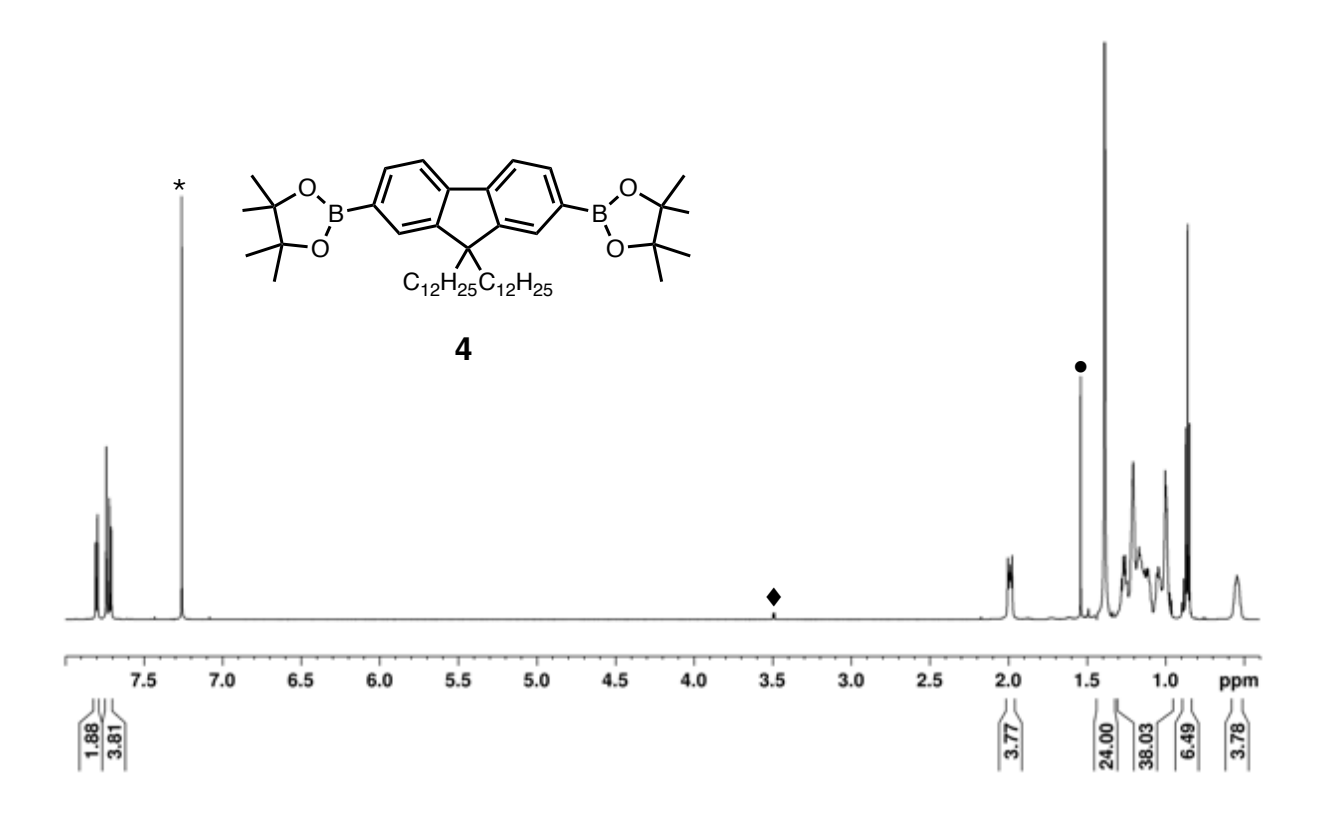


Figure S4. ¹H NMR of compound 4 in CDCl3 (*) where (•) represents water and (♦) represents methanol.

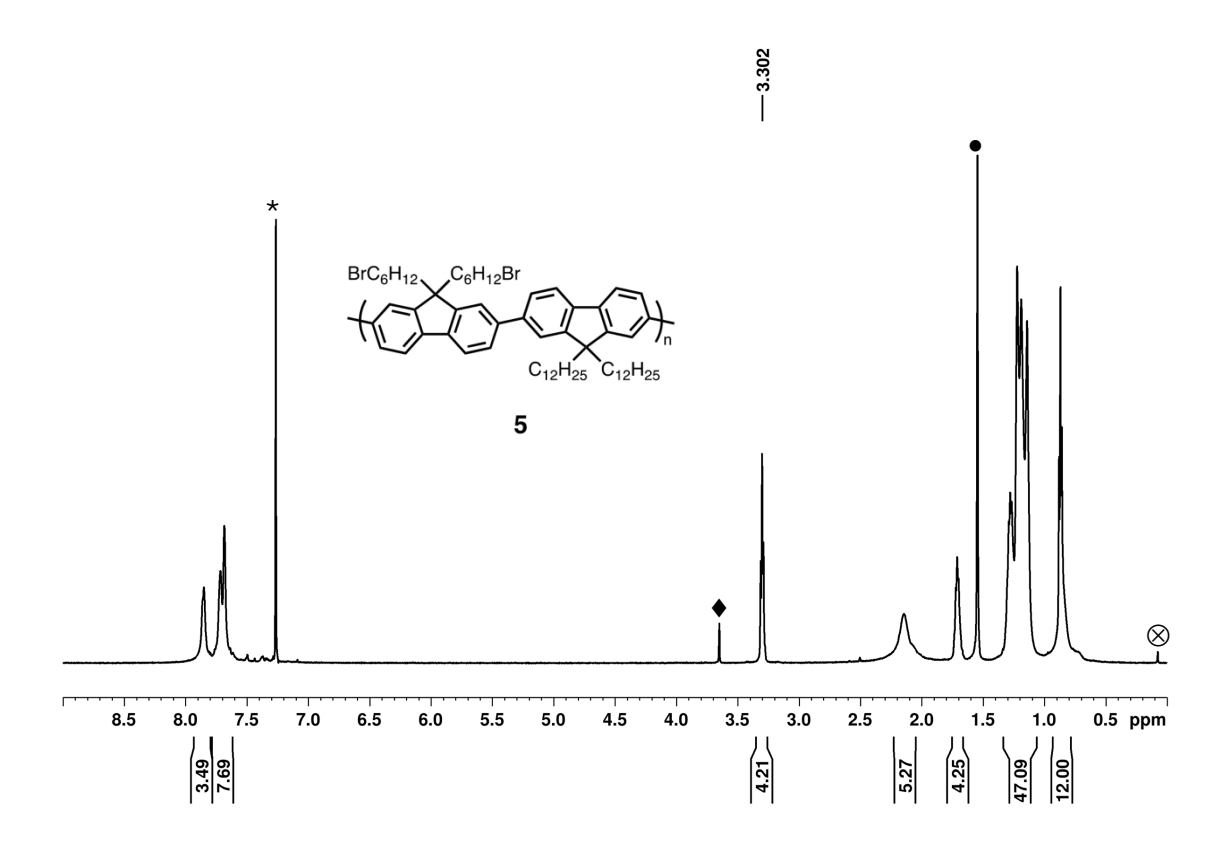


Figure S5. ¹H NMR of compound 5 in CDCl₃ (*) where (\bullet) represents water, (\otimes) silicon grease and (♦) represents methanol.

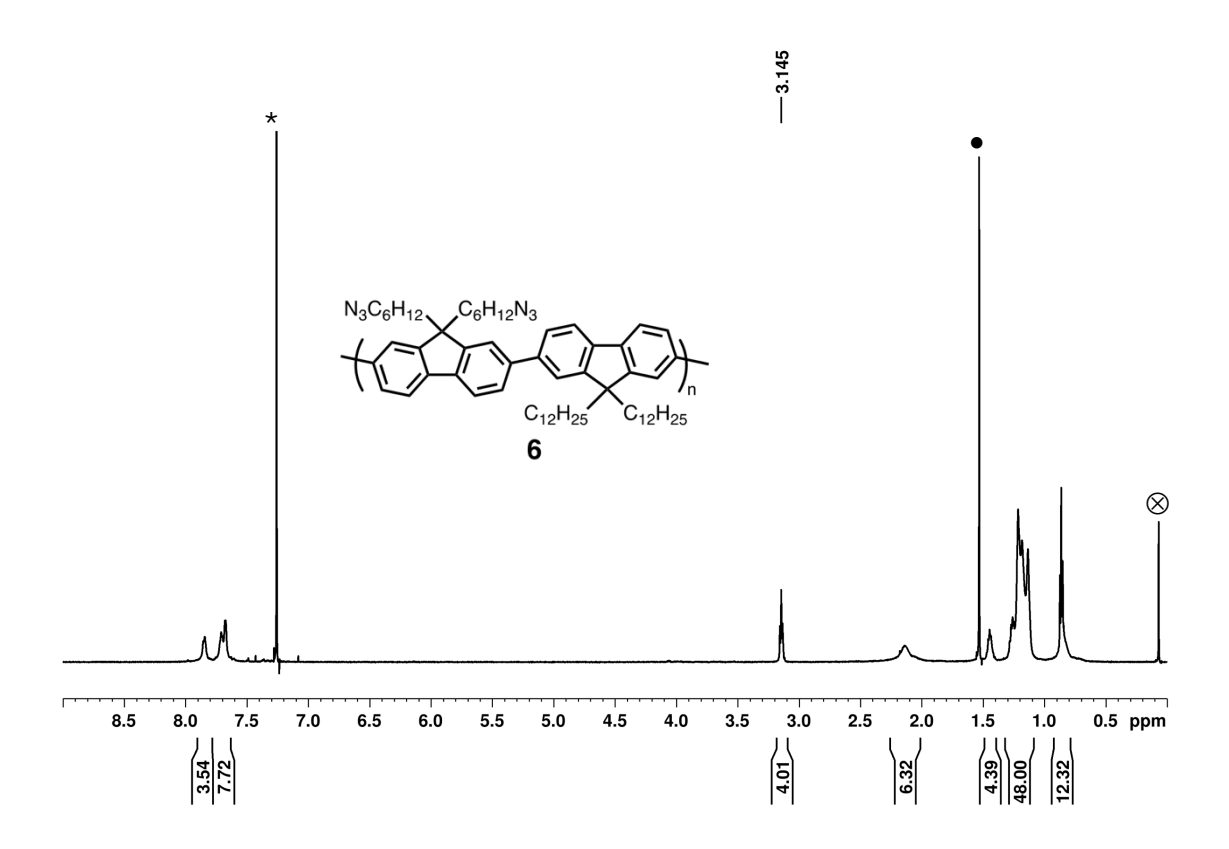


Figure S6. 1H NMR of compound 6 in CDCl $_3$ (*) where (•) represents water, and (\otimes) silicon grease.

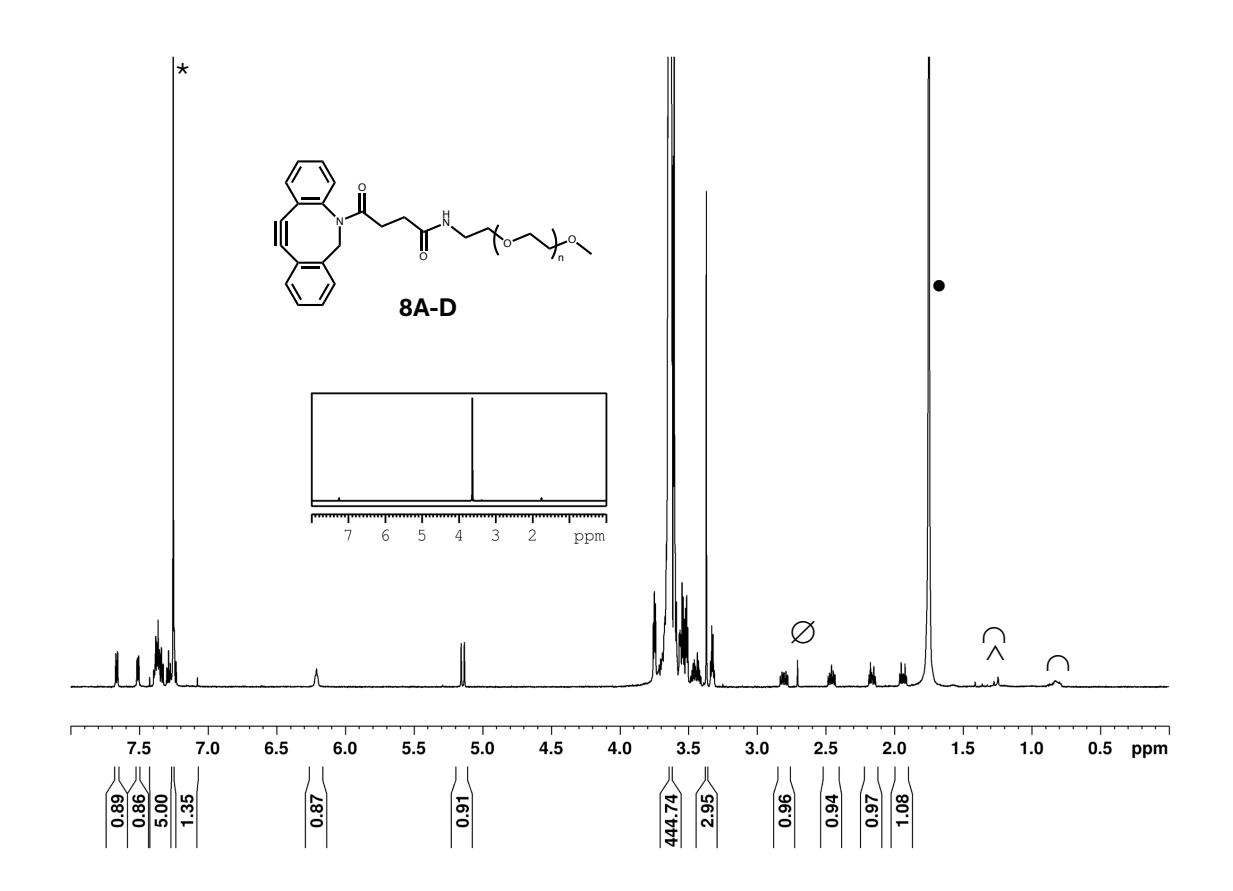


Figure S7. ¹H NMR of Compound 8A (representative of compounds 8B-D) in CDCl₃ (*) where (•) represents water, (\varnothing) N-hydroxysuccinimide, (\wedge) represents diethyl ether and (\cap) represents hexanes. Inset shows the full spectrum without magnification.

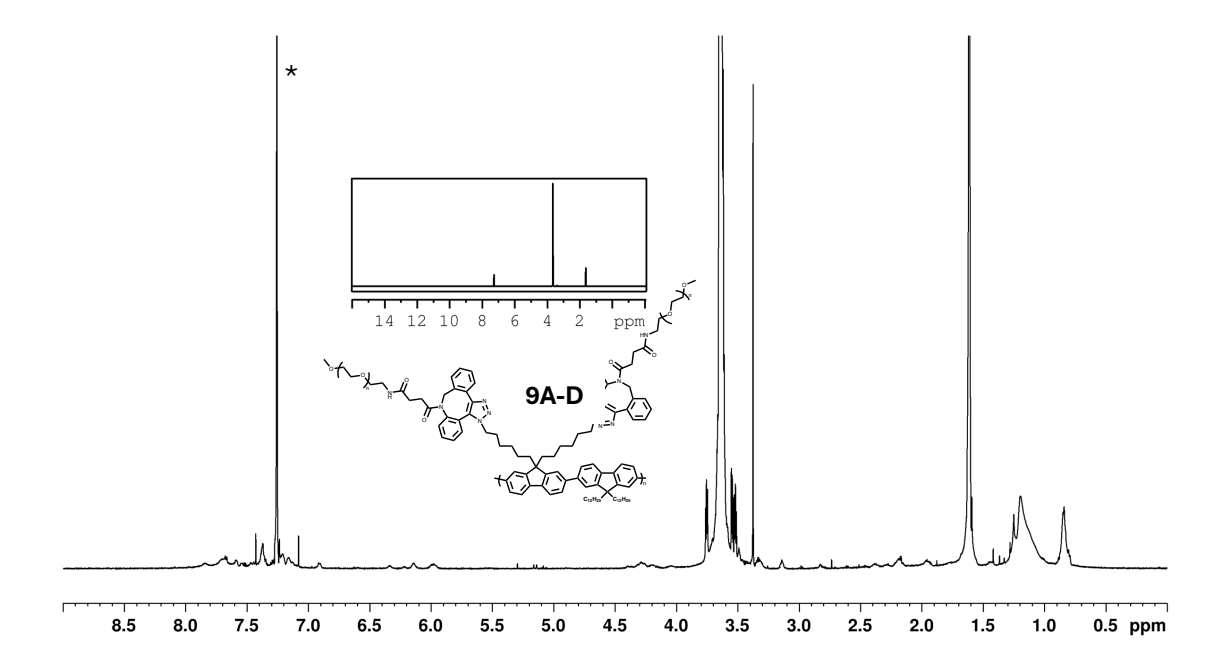


Figure S8. ¹H NMR of Compound 9A (representative for compounds 9B-D) in CDCl₃ (*). Inset shows spectrum without magnification.

A4 Gel Permeation Chromatography (GPC)

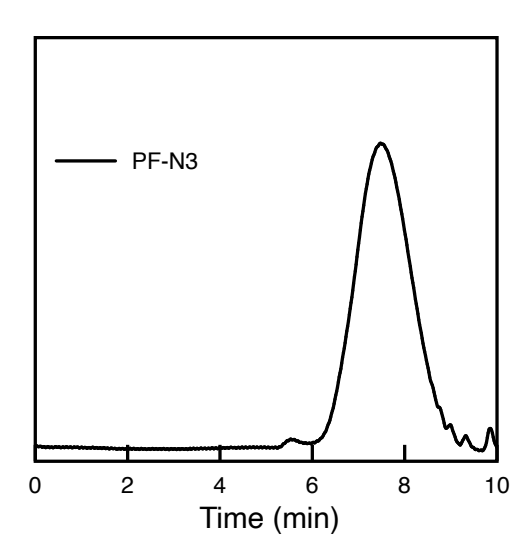


Figure S9. GPC trace of poly(fluorene) (PF-N3).

A5 AFM Images

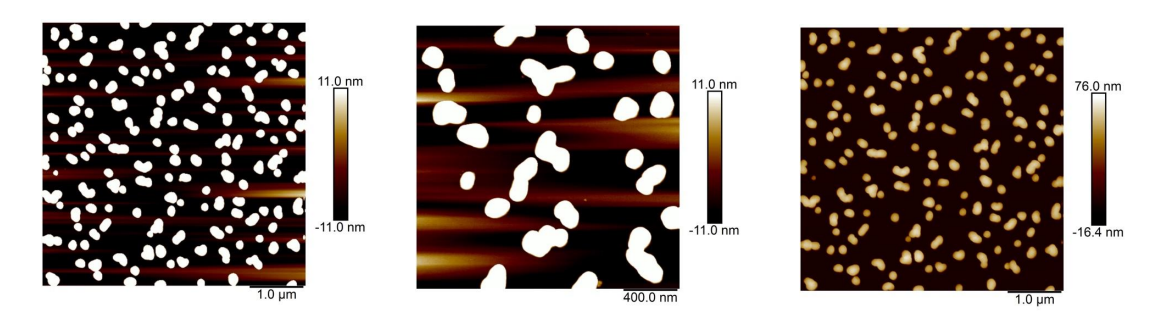


Figure S10. AFM images of PF-N₃ spin-cast onto silicon. Samples were prepared by spincasting 20 μL of a 2mg/2mL in THF onto a silicon substate.

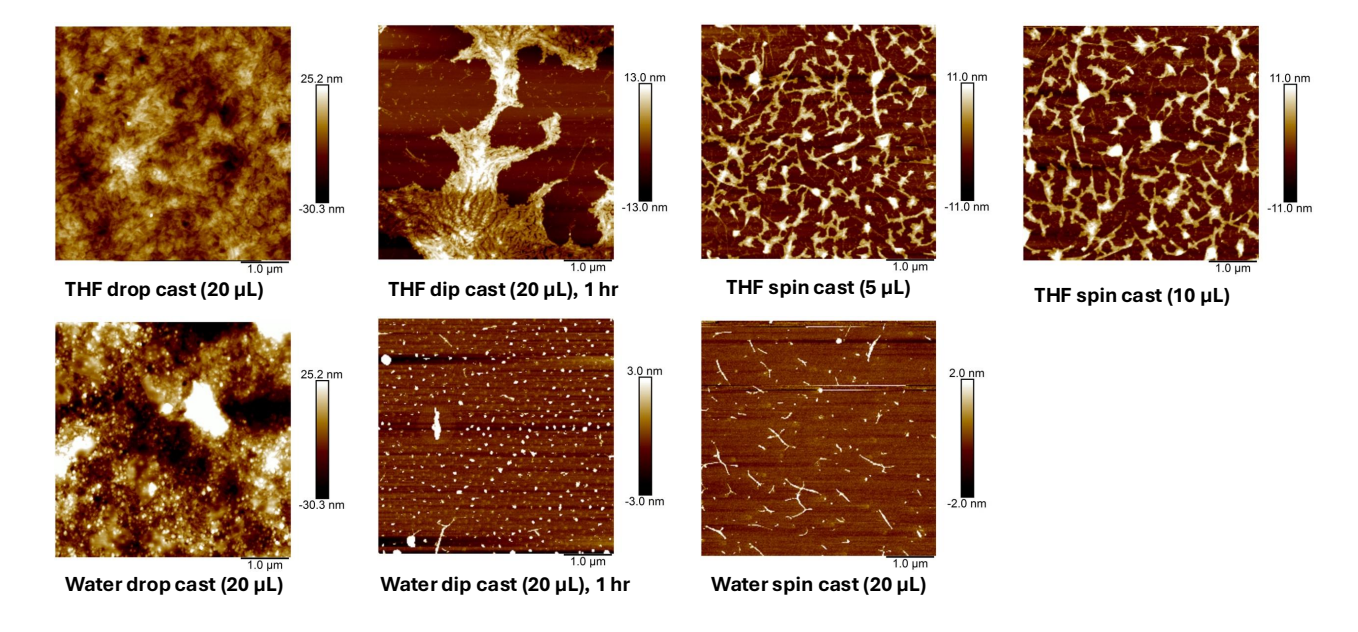


Figure S11. Preliminary AFM images of graft copolymer with 40 kDa side chains. All images are on silicon substrate. Additional sample preparation information outlined under each image.

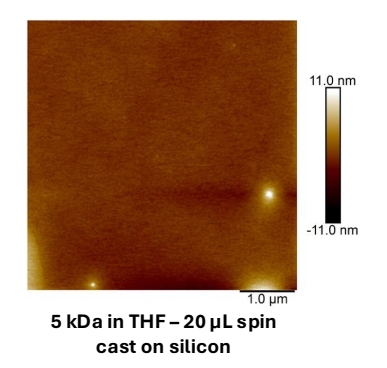


Figure S12. AFM image of 5 kDa dispersion sample in THF spin cast onto silicon substrate.

There are no SWNTs seen in this image.

A6 Calculations

A6.1 Theoretical Calculations for TGA Curves

As detailed by the GPC data, the M_n of the backbone polymer is ~39 kDa. This translates to ~42 repeat units in the backbone with two side chains each: this totals to 84 side chains overall. The molecular weights of the side chains are assumed to be 5, 10, 20 and 40 kDa (ignoring the DBCO small molecule attached). With the 5 kDa side chains, a polymer backbone with molecular weight ~39 kDa will have ~420 kDa of side chains. Therefore, the total M_n of the graft copolymer with the 5 kDa side chains would be ~459 kDa. Of this ~8.5% is the polymer backbone with the rest made up by the side chains.

$$\frac{39,000\,Da}{459,000\,Da} = \frac{x}{100\%}$$

$$\frac{(39,000\,Da)(100\%)}{459,000\,Da} = x$$

$$8.5\% \approx x$$

Calculation 1. Sample calculation for percentage of backbone polymer in graft copolymer with 5 kDa side chains.

In the same way the theoretical percentage of backbone polymer in all other graft copolymers (with differing side chain molecular weights) were calculated.

A6.2 Extinction Coefficient and Mass Calculation of PF-N₃ in Graft Copolymers

To determine the extinction coefficient of PF-N₃ in THF, a standard curve was generated using serial dilutions of PF-N₃ in THF starting from a stock solution of 1mg/10mL (**Figure S13**). Based on the absorbance and concentrations from these dilutions (**Table S1**), a linear plot was created. The equation from the linear trendline was used to determine the extinction coefficient (the slope). This was $55.5 \text{ mL mg}^{-1}\text{cm}^{-1}$.

It should be noted that these calculations represent rough approximations of polymer concentration, without accounting for dispersity in molecular weight. Despite the obvious error associated with these values, the calculations proved useful in approximating the amount of each graft copolymer required to ensure that the backbone concentration was roughly equal in all samples, making them comparable.

Table S1. Tabulated concentrations and absorbances used to generate the trendline.

Sample	Absorbance of Serial Dilution
0.013 mg/mL	0.813
0.0088 mg/mL	0.539
0.0059 mg/mL	0.371
0.0039 mg/mL	0.258
0.0026 mg/mL	0.178

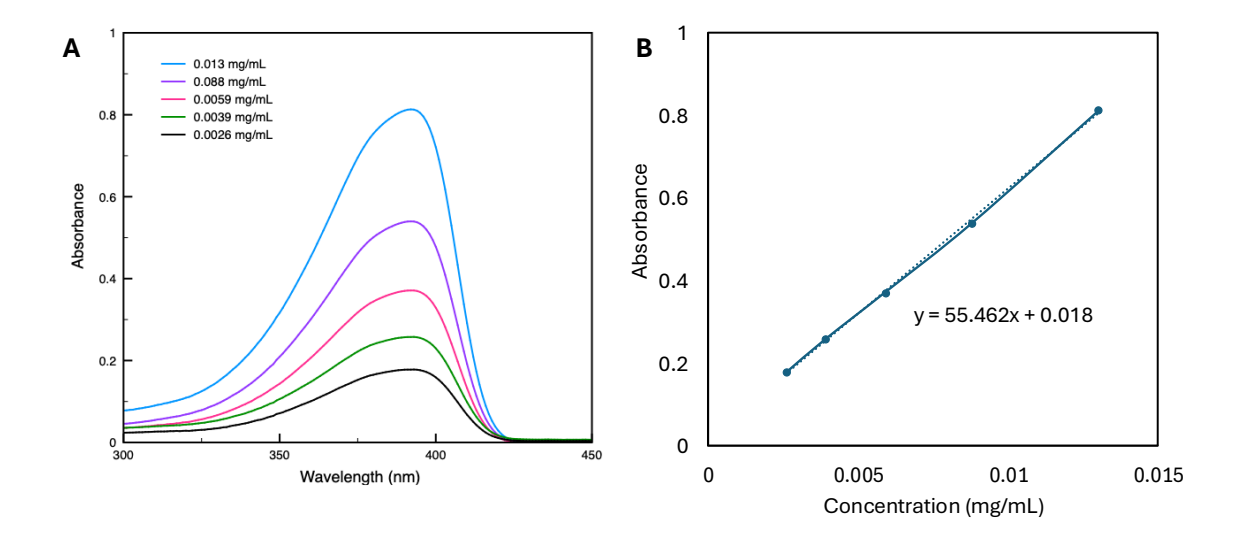


Figure S13. (A) Serial dilutions of PF- N_3 in THF starting with a stock solution of 1mg/10mL. 2mL of each solution was added for a total of 3mL volume in the cuvette for UV-Vis measurements. (B) The resultant standard curve with linear trendline from the serial dilutions.

With the extinction coefficient determined, the Beer Lambert Law can be employed. First, the absorbance of each graft copolymer was identified by UV-Vis spectroscopy (as tabulated in **Table S2** and shown in **Figure 16**).

Absorbance	Calculated Concentration (mg/mL)
0.383	0.0069
0.371	0.0067
0.383	0.0069
0.365	0.0066
	0.383 0.371 0.383

This absorbance was used to determine the concentration of PF- N_3 in each graft copolymer in the cuvette (**Calculation 3**).

$$A = \varepsilon bC$$

$$C = \frac{A}{\varepsilon b}$$

$$C = \frac{0.383}{(55.5 \text{ mL } mg^{-1}cm^{-1}) (1 \text{ cm})}$$

$$C = 0.0069 \text{ mg/mL}$$

Calculation 2. Sample calculation using the 5 kDa graft copolymer for deriving the concentration using the Beer Lambert Law and established extinction coefficient.

Finally, the mass was determined as shown in **Calculation 3** below. Mass of samples, based on equal concentration of PF-N₃, were weighed to be 5 kDa (3 mg), 10 kDa (4.5 mg), 20 kDa (11.2 mg), 40 kDa (24.6 mg). These measured samples were dissolved in 10 mL of THF. From this stock solution, 300 μ L was added to the cuvette for a total volume of 2 mL.

$$C_1 V_1 = C_2 V_2$$

$$\left(0.0069 \frac{mg}{mL}\right) (2 mL) = C_2 (10 mL)$$

$$C_2 = 0.00138 \frac{mg}{mL}$$

$$m = (10 mL) \left(0.00138 \frac{mg}{mL}\right) = 0.0138 mg$$

Calculation 3. Determination of the mass of PF-N3 in each graft copolymer sample.

Table S3. Tabulated calculated masses of PF-N₃ in each sample of graft copolymer in THF.

Sample	Calculated Mass (mg)
5 kDa	0.0138
10 kDa	0.0134
20 kDa	0.0138
40 kDa	0.0132